[Frontiers In Bioscience, Landmark, 23, 1902-1922, June 1, 2018]

Investigation of the structure and dynamic of calmodulin-nitric oxide synthase complexes using NMR spectroscopy

Michael Piazza[1], Thorsten Dieckmann[1] Joseph Guy Guillemette[1]

[1]Department of Chemistry, University of Waterloo, Waterloo, Ontario N2L 3G1, Canada

TABLE OF CONTENTS

1. ABSTRACT

NMR spectroscopy allows for the determination of high resolution structures, as well as being an efficient method for studying the dynamics of protein-protein and protein-peptide complexes. ^{15}N relaxation and H/D exchange experiments allow for the analysis of these structural dynamics at a residue specific level. Calmodulin (CaM) is a small cytosolic Ca^{2+} binding protein that serves as a control element for many enzymes. An important target of CaM are the nitric oxide synthase (NOS) enzymes that play a major role in a number of key physiological and pathological processes. Studies have shown CaM facilitates a conformational shift in NOS allowing for efficient electron transfer through a process thought to be highly dynamic and at least in part controlled by several possible phosphorylation sites. This review highlights recent work performed on the CaM-NOS complexes using NMR spectroscopy and shows remarkable differences in the dynamic properties of CaM-NOS complexes at physiologically relevant Ca^{2+} concentrations. It also shows key structural changes that affect the activity of NOS when interacting with apoCaM mutants and NOS posttranslational modifications are present.

2. INTRODUCTION

2.1. Protein high-resolution NMR spectroscopy

Nuclear magnetic resonance (NMR) spectroscopy is one of the main methods used to determine high resolution three-dimensional (3D) structures of proteins, comparable to those determined by X-ray crystallography, and to monitor protein-ligand interactions and internal dynamics of a protein (1–3). NMR spectroscopy is also used to determine structures of proteins and molecules that cannot be crystallized due to their high flexibility and mobility. The determination of large protein structures is a limitation of NMR spectroscopy because of chemical shift overlap and lower sensitivity due to the fast decay of the NMR signal (4). For NMR studies, proteins require the incorporation of isotopes, specifically ^{15}N and ^{13}C, which are costly (3,5,6). For studies of complexes, ideally both partner proteins should be available in isotope labeled forms.

The first step in an NMR based structure determination is to completely assign the ^{1}H, ^{15}N, and ^{13}C NMR spectra of the protein, followed by the assignment of as many nuclear Overhauser

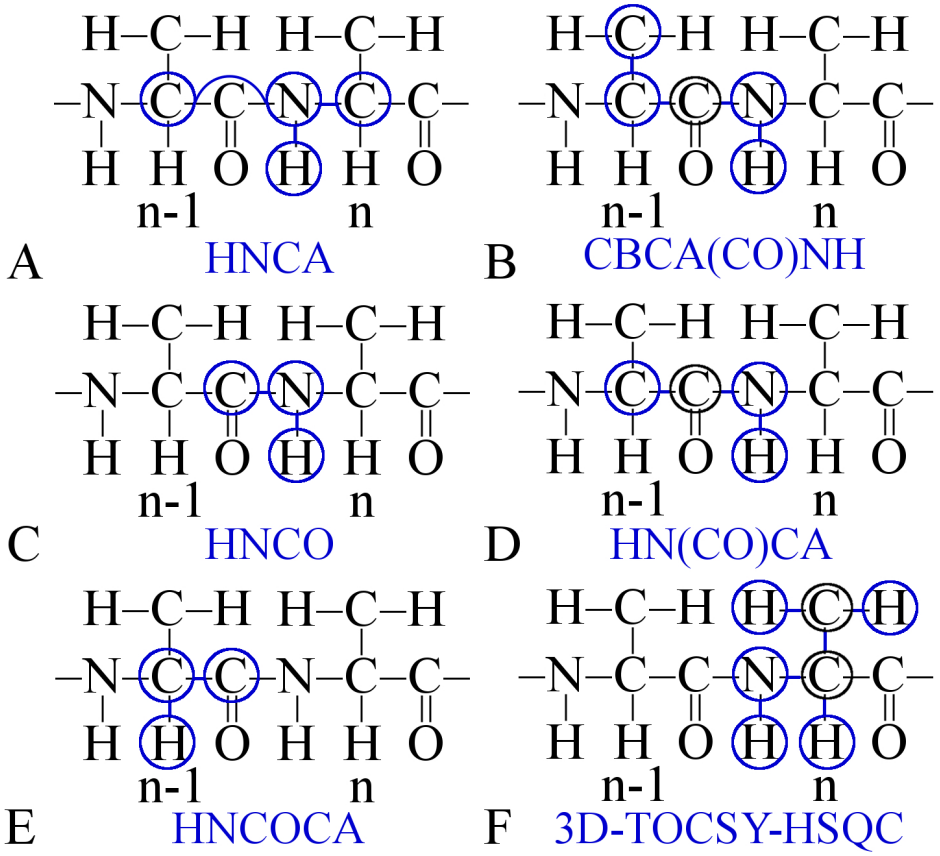

Figure 1. Heteronuclear multidimensional NMR experiments used for resonance assignments of proteins. NMR experiments used to make resonance assignments for ^{1}H, ^{13}C and ^{15}N nuclei in a protein (3). This is done by the transfer of magnetization through bonds, shown by blue lines, to different nuclei, shown by blue circles. (A) HNCA-3D experiment which correlates the ^{15}N and NH chemical shifts with the intraresidue and preceding residue Cα shift (13). (B) CBCA(CO)NH-3D experiment which correlates the ^{15}N and NH chemical shifts with the preceding residue Cα and Cβ shift (14). (C) HNCO-3D experiment which correlates the ^{15}N and NH chemical shifts with the preceding residue carbonyl shift (13). (D) HN(CO)CA-3D experiment which correlates the ^{15}N and NH chemical shifts with the preceding residue Cα shift (15). (E) HCACO which correlate the carbonyl shift the intraresidue Cα and Hα shifts (13). (F) 3D-TOCSY (TOtal Correlation SpectroscopY) HSQC-3D experiment which correlates the ^{15}N and NH chemical shifts with the side chain ^{1}H shifts (16).

enhancement (NOE) interactions as possible (7,8). These provide the principal information necessary for determining the 3D structure of a protein. The NOE is correlated with the distance between hydrogen atoms in the protein and thus can provide a set of internuclear distance constraints. NOEs are due to the dipolar coupling, through-space, between nuclei, in which the local field at one nucleus is influenced by the presence of the other nucleus (8). The larger the number of NOE constraints that can be determined, the higher the precision of the structure.

The problem with the assignment of larger proteins is the severe overlap of resonances and the increased line widths of the NMR signals which is caused by the slower tumbling of large molecules in solution. One way to address these problems is the isotopic labelling of the sample and the use of 2D and 3D heteronuclear NMR (3,9,10). 2D experiments are used to measure the correlation of two resonance frequencies through-bond or through-space (1). The same principle can be extended to higher dimensional spectra. The use of 3D and 4D experiments have aided in overcoming the problem of overlapping peaks by expanding the 2D spectrum into additional dimensions, allowing these overlapping areas to be separated into layers (11).

One of the key spectra used in structure determination is the ^{1}H-^{15}N-heteronuclear single quantum correlation (HSQC) experiment (12). This experiment correlates each proton to a directly attached nitrogen atom in the protein. This includes the all backbone amides except proline, and the side chain amides. This spectrum provides the “finger print” of the protein, typically giving rise to one peak for each amino acid other than proline in the protein. Assignment of these peaks to specific residues in the protein cannot be done using the ^{1}H-^{15}N-HSQC alone, and other 3D experiments must be performed (Figure 1). Heteronuclear multidimensional NMR experiments are used for resonance assignments of proteins (3).

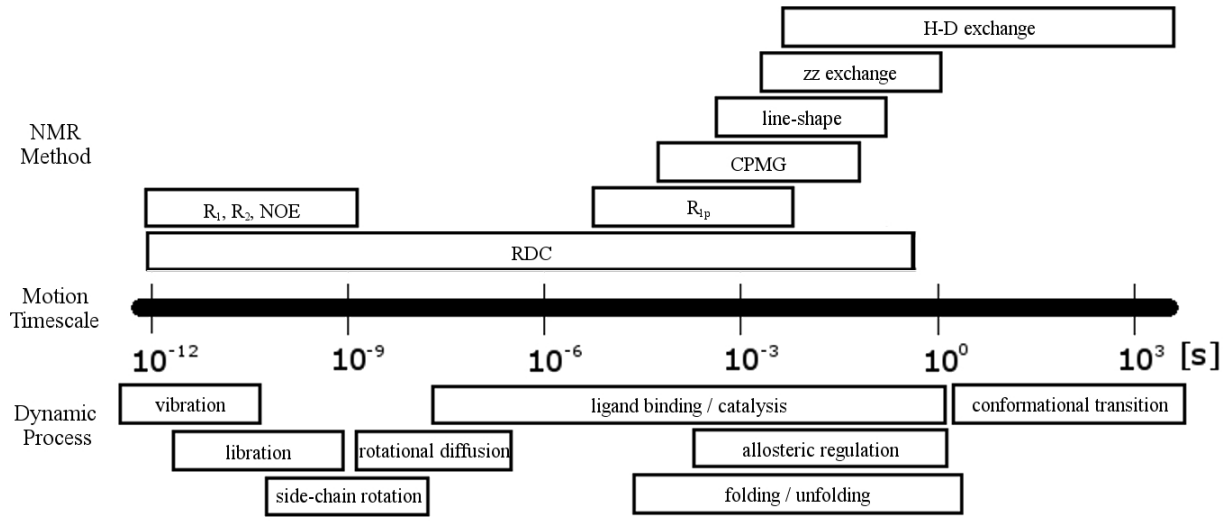

Figure 2. Time scales of various dynamic processes found in proteins and NMR method used to determine them (6,18,19).

These experiments include the HNCA (13), CBCA(CO)NH (14), HNCO (13), HN(CO)CA (15), HCACO (13) and 3D-TOCSY (TOtal Correlation SpectroscopY) HSQC (16).

2.2. NMR methods for studying protein dynamics

In addition to 3D structures, NMR spectroscopy can also provide quantitative information on molecular dynamics of protein systems at a residue specific level. These studies provide direct evidence of structural changes and intramolecular dynamics associated with functions that are central to understanding the role of dynamics in protein function (6,17–21). By tracking chemical shift changes, NMR spectroscopy is able to characterize very weak interactions between proteins and ligands at atomic (or residue) levels (22,23). Others methods for characterizing weak interactions of protein complexes are relaxation dispersion and paramagnetic relaxation enhancement, which allow the detection and visualization of low populated states of these complexes (24,25). NMR spectroscopy can also provide information about conformational dynamics and exchange processes of biomolecules at timescales ranging from picoseconds to seconds, and is very efficient in determining ligand binding and mapping interaction surfaces of protein/ligand complexes as shown in Figure 2 (18,19).

2.2.1. Amide exchange experiments

Detailed information about fluctuations in protein structures and site-specific information on the stability of secondary structural elements can be obtained from the measurement of amide proton (NH) hydrogen/deuterium exchange (H/D) rates using NMR spectroscopy (26–28). An alternate method for studying H/D exchange is using mass spectrometry (29,30). These fluctuations expose some of the NH to the D_2O solvent, thus facilitating the NH/ND exchange process while other amide protons remain protected from exchange. The exchange rate of NH groups in proteins is determined by a combination of their intrinsic exchange rate in the absence of secondary structure and the presence of secondary structure and solvent inaccessibility that protect from exchange (31,32). H/D exchange experiments are also useful for accessing the stability of specific structure elements within a protein or protein complex (33,34).

2.2.2. ^{15}N relaxation experiments

Information about residue specific internal dynamics on the fast, picosecond to nanosecond, timescale is determined primarily from model-free analyses (19,35). This is accomplished through the analysis of longitudinal (T_1) and transverse (T_2) relaxation, as well as heteronuclear NOEs (36). This allows internal motions such as bond vibrations and librations to be interpreted through the determination of order parameters (S^2) and internal effective correlation times (τ_e) by the “model free” approach (35). These parameters quantitatively describe the magnitude and time scale of local, intramolecular motions and thus allow one to correlate molecular dynamics with biological function. The model-free approach characterizes backbone mobility using an order parameter S^2, which may be interpreted as the amplitude of the motion, and a correlation time, τ_i, which is the characteristic time constant of this motion (6,37,38). The relaxation analysis is termed model free because the order parameters determined have model independent significance.

3. INVESTIGATION OF NOS PEPTIDE-CAM INTERACTIONS USING DIFFERENT NMR TECHNIQUES

Calmodulin (CaM) is a small cytosolic Ca^{2+}-binding protein that is ubiquitous in eukaryotic cells. It is able to bind and regulate hundreds of different intracellular proteins (39). CaM consists of two globular domains connected by a flexible central linker region. Each globular domain contains two EF hands that are each capable of binding one Ca^{2+} ion. The EF hand consists of a helix−loop−helix motif, containing a 12 residue long Ca^{2+} binding loop rich in aspartates and glutamates (40). In the Ca^{2+}-deplete form the helix−loop−helix motif of the EF hand is in a "closed" conformation, with their hydrophobic residues packed into their central core and their charged, hydrophilic residues solvent-exposed (41,42). When a Ca^{2+} ion binds, the helices rearrange into a more "open" conformation, exposing hydrophobic patches in each domain that allow CaM to bind to bind and activate its intracellular target proteins (40,41,43). The binding of Ca^{2+} to CaM is cooperative within each lobe of CaM but not between the lobes, with the C-lobe of CaM able to bind Ca^{2+} with a ten-fold higher affinity than the N-lobe (44,45). The flexibility of CaM's central linker allows it to adapt its conformation to optimally associate with its intracellular targets. CaM is able to bind to its target proteins in the Ca^{2+}-replete and Ca^{2+}-deplete forms.

The nitric oxide synthase (NOS) enzymes (E.C. 1.1.4.1.3.3.9), which catalyze the production of nitric oxide (•NO), are one of the most studied target proteins bound and regulated by CaM (46). There are three NOS isoforms in mammals: neuronal NOS (nNOS), endothelial NOS (eNOS), and inducible NOS (iNOS). The NOS enzymes are homodimeric with each monomer possessing an *N*-terminal oxygenase domain (containing binding sites for heme, tetrahydrobiopterin (H_4B), and the substrate L-arginine) and a *C*-terminal reductase domain (containing binding sites for the cofactors FMN, FAD, and NADPH) connected by a CaM binding domain (46,47). The CaM binding domain of all three NOS isoforms contain the classical 1-5-8-14 CaM-binding motif, with CaM binding in an antiparallel fashion (48,49). CaM binds to iNOS regardless of intracellular Ca^{2+} concentration and is fully active at basal levels of Ca^{2+} (<100 nM) in the cell (50–53), whereas CaM's interaction with the constitutive NOS enzymes (eNOS and nNOS) is Ca^{2+}- dependent, requiring 200-300 nM concentrations of free Ca^{2+} to achieve half maximal activity (54,55).

Electron flow in the NOS enzymes proceeds from the NADPH, through the FAD and FMN cofactors, to the heme oxygenase domain. Recent studies suggests a dimerized oxygenase domain acts as the anchoring dimeric structure for the entire NOS enzyme. This anchoring dimeric structure is flanked by two separated reductase domains that exist in an equilibrium of conformations that alternate between FAD-FMN electron transfer and FMN–heme electron transfer. CaM binding induces a shift in the conformational equilibrium allowing for efficient electron transfer (56–61). When CaM is fully bound to NOS, residues of CaM's N-lobe interact with the FMN subdomain of NOS and form a bridge interaction that appears necessary to control the interaction between the FMN and heme, (62). This bridge interaction enables CaM to activate NOS through the stabilization and precise positioning of the FMN subdomain for the shuttling of electrons from the FMN to the oxygenase domain. Clearly, these conformational changes caused by CaM are important in stimulating efficient electron transfer within the NOS enzymes.

Understanding the structural basis of CaM's target protein interactions and diverse regulatory functions is crucial for rationalizing and developing strategies for controlling the regulation pathways for medical purposes. CaM's interactions with the various NOS isozymes have previously been studied by NMR (63–67). This review highlights the recent work performed on the CaM-NOS complexes using NMR spectroscopy. It will show the remarkable differences in the dynamic properties of CaM-NOS complexes at the residue level when experiments performed at physiologically relevant nanomolar Ca^{2+} concentrations are compared to those performed at high millimolar Ca^{2+} concentrations. It will also show key structural changes that affect the activity of NOS when common apoCaM mutants and NOS posttranslational modifications are used.

3.1. NMR spectroscopy at physiological Ca^{2+} concentrations

NMR spectroscopy has previously been used to study CaM's interaction with various NOS isoforms (63–67). However, most structural and dynamics studies on CaM-NOS interactions have been performed at non-physiological conditions, which do not represent the true intracellular Ca^{2+} concentration, using either apo (Ca^{2+} free with excess chelators, such as EDTA, present) or Ca^{2+} saturated (greater than 1mM Ca^{2+}) conditions. NMR experiments performed at free Ca^{2+} concentrations that are in the resting intracellular Ca^{2+} concentration range of less than 100 nM (52,53), and at elevated intracellular Ca^{2+} concentrations of 225 nM as well as under saturation conditions (1 mM) provide further insights into the structure and dynamics of the CaM-NOS interaction. At resting intracellular Ca^{2+} concentrations, CaM is unable to bind to the eNOS CaM-binding domain peptide. The minimal free Ca^{2+} concentration needed for CaM to interact with eNOS was determined to be 225 nM (68). The NMR structure at a physiological free Ca^{2+} concentration of 225 nM shows the CaM-eNOS complex has a C-terminal lobe

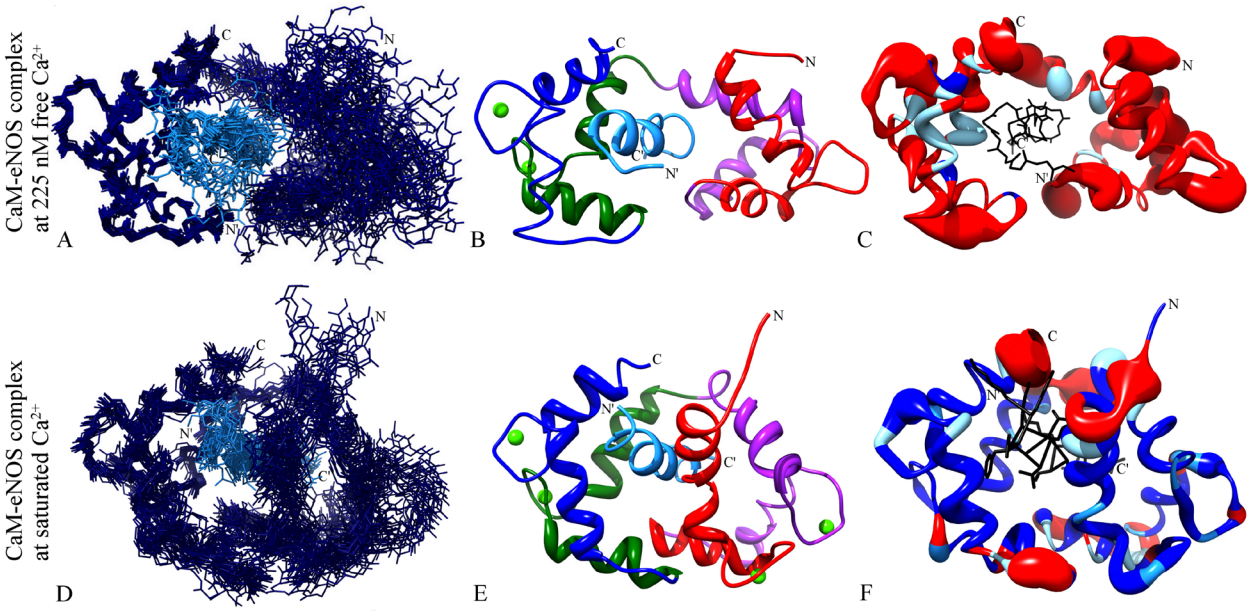

Figure 3. Solution structure of CaM-eNOS at 225 nM Ca^{2+}. Superposition of the ensemble of the 20 lowest-energy calculated NMR solution structures of (A) CaM bound to eNOS peptide at 225 nM Ca^{2+} (PDB 2N8J) and (D) the previously determined solution structures of CaM bound to eNOS peptide at saturated Ca^{2+} (PDB 2LL7). The superposition is aligned by the backbone atoms of the C-lobe of CaM. Backbone atom traces of CaM are colored dark blue, and the eNOS peptide colored light blue. Cartoon ribbon view of the average solution structure of the CaM− eNOS complex at (B) 225 nM Ca^{2+} and (E) saturated Ca^{2+}. Residues 1−40 of CaM (EF hand I) are colored red, residues 41−79 (EF hand II) purple, residues 80−114 (EF hand III) green, and residues 115−148 (EF hand IV) blue. The peptide is colored lighter blue. Calcium ions are colored green. Worm models of CaM-eNOS peptide complex at (C) 225 nM Ca^{2+} and (F) saturated Ca^{2+} illustrating their internal dynamics and amide H/D exchange data. The worm radius ranges from 0.2.5 (S^2 value of 1), to 4 (S^2 value of 0.4.). Residues that display fast D_2O exchange rates are colored red on the ribbon structure. Residues that display intermediate D_2O exchange rates are colored light blue and residues that display slow D_2O exchange rates are colored blue. The bound peptide is colored black and shown in wire form. The images were created using Chimera.

that is structurally similar to the Ca^{2+}-replete CaM-eNOS complex, and an N-terminal lobe structurally similar to unbound, apoCaM (68,69).

The family of twenty lowest energy structures is shown in Figure 3A. The alignment of the 20 lowest energy structures show the C-lobes of CaM superimpose quite well with each other, whereas the N-lobe has a lot of fluctuation in its relative position to the C-lobe, suggesting a less rigid and more dynamic N-lobe. When a similar comparison is made with the 20 lowest energy structures for the Ca^{2+} saturated CaM-eNOS complex (Figure 3D) superposition via both the C- and N-lobes results in well overlaid structures. The r.m.s.d. values for the individual lobes of CaM also show a more dynamic N-lobe in the CaM-eNOS complex structure at 225 nM free Ca^{2+}. The r.m.s.d. for the C-lobe backbone atoms is 0.6. Å, whereas it is 0.9. Å for the N lobe backbone atoms. The CaM-eNOS complex structure at 225 nM free Ca^{2+} has a Ca^{2+}-replete C-lobe bound to the eNOS peptide and a Ca^{2+} free N-lobe loosely associated to the eNOS peptide (Figure 3B). The N-terminus of the eNOS peptide displays an α-helical secondary structure, whereas the C-terminus displays a less α-helical secondary structured region due to having a weaker interaction with CaM. Comparing to the Ca^{2+} saturated CaM-eNOS complex structure (Figure 3E) one can see that the N-lobe at 225 nM free Ca^{2+} has a much looser association to the eNOS peptide.

3.1.1. Structure and dynamics comparison to saturating Ca^{2+} structure

The 225 nM free Ca^{2+} and Ca^{2+} saturated CaM-eNOS complex structures offer an interesting case for comparison (Figure 4A,B). This comparison shows that the C-lobes of CaM and peptide orientation are similar, whereas the N-lobe is structurally different. When the two structures are aligned with respect to CaM's C-lobe backbone atoms the eNOS peptide and the C-lobes of CaM of each structure superimpose quite well on each other (r.m.s.d. value of 1.0.23 Å), whereas the N-lobes of CaM do not. When the 225 nM free Ca^{2+} CaM-eNOS complex structure is compared to the previously determined apoCaM structure (PDB entry 1CFC), there is structural similarity of the N-lobes of CaM, and differences between the C-lobes of CaM (Figure 4C,D). When the two structures are aligned with respect to CaM's N-lobe backbone atoms the N-lobes of CaM of each structure superimpose well on each other (r.m.s.d. value of 1.0.42 Å), whereas the C-lobes of CaM do not.

The dynamic properties of these complexes examined by amide H/D exchange time-course and

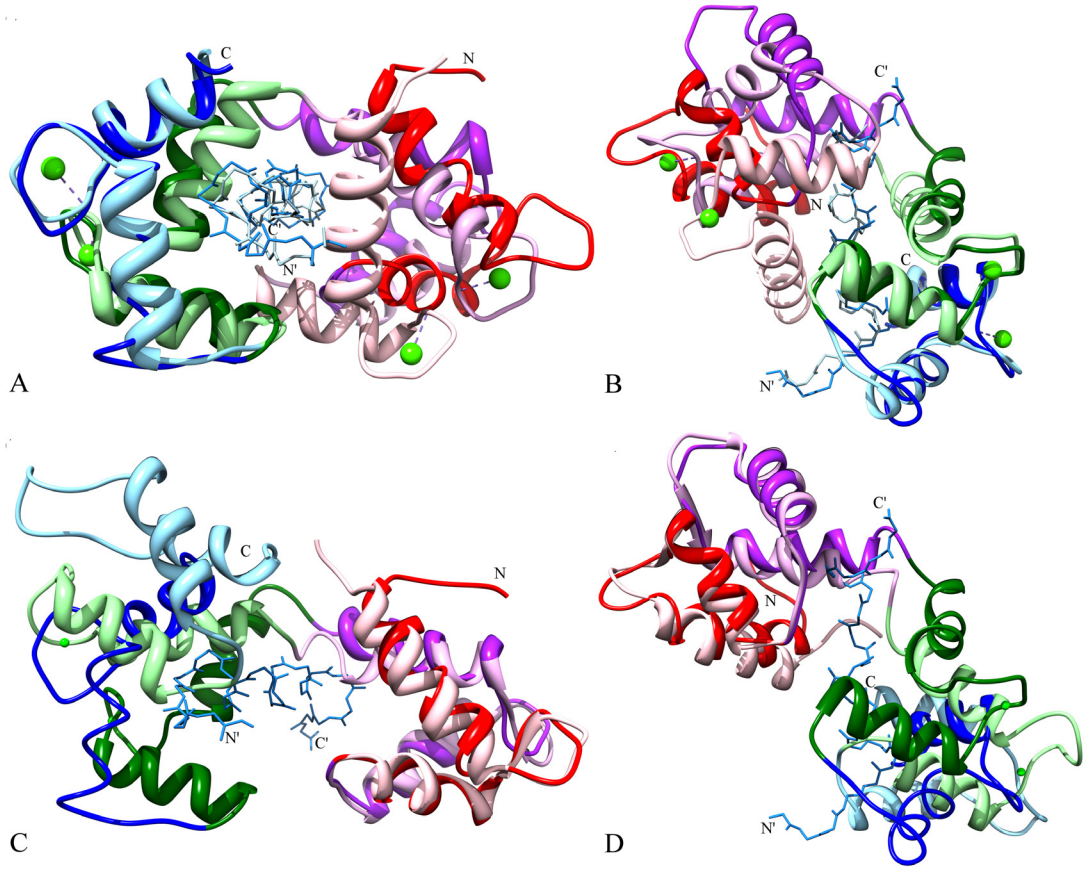

Figure 4. Comparison of the solution structure of the CaM-eNOS peptide complex at 225 nM Ca^{2+} (PDB 2N8J) with the solution structures of saturated Ca^{2+} CaM-eNOS peptide complex (PDB 2LL7) and apoCaM (PDB 1CFD). The solution structures of the CaM−eNOS peptide at 225 nM Ca^{2+} (dark colors) and at saturated Ca^{2+} (light colors) are aligned by superimposition of the backbone atoms of the C-lobes of CaM (A) viewed along the bound peptide from its N-terminus (N′) to its C-terminus (C′) and (B) rotated around the horizontal axis with the C-terminus of the bound peptide on the top. The solution structures of the CaM−eNOS peptide at 225 nM Ca^{2+} (dark colors) and apoCaM (light colors) are aligned by superimposition of the backbone atoms of the N-lobes of CaM (C) viewed along the bound peptide from its N-terminus (N′) to its C-terminus (C′) and (D) rotated around the horizontal axis with the C-terminus of the bound peptide on the top. Residues 1−40 of CaM (EF hand I) are colored red, residues 41−79 (EF hand II) purple, residues 80−114 (EF hand III) green, and residues 115−148 (EF hand IV) blue. The peptide is colored lighter blue. The broken lines connect the Ca^{2+} ion to the structure it was determined from. Reprinted with permission from Biochemistry, 55, Piazza M, Dieckmann T, Guillemette JG. Structural Studies of a Complex Between Endothelial Nitric Oxide Synthase and Calmodulin at Physiological Calcium Concentration, 5962–5971, Copyright (2016) American Chemical Society. The images were created using Chimera.

NMR ^{15}N relaxation experiments agree very well with the determined solution structures (68). At 225 nM free Ca^{2+} the amides from residues in the N-lobe of CaM exhibited fast H/D exchange and higher internal dynamics, while residues in the C-lobe of CaM were protected from exchange, with most of those exhibiting intermediate exchange and lower internal dynamics (Figure 3C,F). M36, M51, M72 and K75 of the N-lobe exhibit intermediate exchange and are all found to be part of α-helices and have hydrophobic interactions with L509, one of the anchoring residues of eNOS, in the solution structure of the complex. This suggests that even though this lobe is Ca^{2+} free and not tightly bound to the peptide it is still maintaining its structural integrity and might also maintain some transient interactions with the peptide. Residues V91, F92, L105, L112, F141 and M144 of the C-lobe of CaM show intermediate or slow exchange and interact via hydrophobic interactions with the other anchoring residues F496, A500 and V503 of the eNOS peptide. The lower overall dynamics of the C-lobe of CaM compared to the N-lobe correspond well with the more rigid C-lobe observed in the structure at 225 nM free Ca^{2+}. The structure and dynamics data show that the residues of CaM interacting with eNOS' 1-5-8-14 anchoring residues (Table 1) have a strong interaction at 225 nM free Ca^{2+} concentration, which keeps the complex bound, while the rest of the residues of the CaM protein are able to fluctuate or "breathe". Comparing the two lobes of CaM, the residues of the C-lobe display a more rigid structure (lower r.m.s.d., lower degree of internal mobility (higher S^2) and higher exchange protection), indicating a stronger interaction with the N-terminal region of the eNOS peptide to hold the complex together and induce an α-helical structure. Whereas the N-lobe of CaM is

Table 1. The sequences of the iNOS, eNOS and nNOS CaM binding regions with the anchor residues indicated

NOS isoform	CaM binding domain residues	Residue number in full length NOS
nNOS	RRAIG **F**KKL**A** EA**V**KF SAKL**M** GQ[1]	731-752
eNOS	TRKKT **F**KEV**A** NA**V**KI SASL**M** GT[1]	491-512
iNOS	RREIP **L**KVL**V** KA**V**LF ACML**M** RK[1]	510-531

[1]1, 5, 8, 14 anchoring residues in bold.

more dynamic (increased backbone mobility, less rigid N-lobe and higher r.m.s.d.) and loosely associated with the less structured C-terminal region of the eNOS peptide. At saturating Ca^{2+} concentrations, the entire CaM-eNOS complex has become more rigid, or structurally stable.

In summary, the CaM-eNOS structures demonstrate that CaM bound to the NOS holoenzymes exists in multiple conformations with the most populated state corresponding to CaM docked to the oxygenase domain and having a more highly dynamic N-lobe of CaM is consistent with the proposed conformational sampling of the FMN subdomain (56–61).

These structures suggests that the C-lobe of CaM first binds to the N-terminus of eNOS' CaM-binding domain and possibly part of the heme domain, while loosely associating to the C-terminus of eNOS' CaM-binding domain when the intracellular Ca^{2+} concentration is elevated to 225 nM. In this dynamic state, the less structured C-terminal region of the eNOS CaM binding domain would allow the FMN subdomain to have the flexibility to exist in a complex distribution of conformational states, correlating well with the dynamic N-lobe of CaM observed at 225 nM Ca^{2+}. As the intracellular Ca^{2+} concentration increases (Dansyl-CaM studies suggest 1 μM (68)) the N-lobe then binds Ca^{2+} and becomes tightly bound to the C-terminus of eNOS' CaM-binding domain, allowing for the possibility of a bridge to form between CaM and the FMN domain, which would induce a shift to the FMN-heme electron transfer conformation to allow efficient electron transfer in the NOS enzymes.

When a similar comparison is made using the CaM-iNOS complex, ^{1}H-^{15}N HSQC spectra performed at various free Ca^{2+} concentrations, ranging from resting intracellular Ca^{2+} levels to elevated Ca^{2+} levels, indicate that the CaM-iNOS complex maintains structural integrity at all Ca^{2+} levels. This suggests that CaM adopts the same structure as observed in the Ca^{2+}-replete CaM-iNOS complex when it is bound to the iNOS peptide at free Ca^{2+} levels representative of resting intracellular Ca^{2+} levels (17 nM and 100 nM Ca^{2+}) to elevated Ca^{2+} levels (225 nM Ca^{2+}). This observation is plausible because CaM interacts with iNOS in a Ca^{2+}-independent manner.

The analysis of the internal dynamics between the CaM-iNOS complex at 225 nM free Ca^{2+} concentration and saturating Ca^{2+} agrees well with the results found for the H/D exchange experiments. As determined for the CaM-eNOS complex at saturating Ca^{2+}, the CaM-iNOS complex at saturating Ca^{2+} displays low internal dynamics, slow H/D exchange and overall high stability with the exception of the residues of the linker region and the loop regions between the EF hand pairs (Figure 5). At 225 nM free Ca^{2+} concentration the EF hands and loop regions of the CaM-iNOS complex display fast H/D exchange and faster internal motions observed. This indicates that the coordination of the Ca^{2+} ions by the residues of the EF Hand loop is a weaker interaction compared to that at saturating Ca^{2+} concentrations. The data shows that the residues of CaM interacting with the 1-5-8-14 anchoring residues of iNOS (Table 1) have a strong interaction at low Ca^{2+} concentrations, while the rest of the residues of CaM display increased dynamics and less exchange protection. Specifically, residues of CaM's N-lobe have a lower degree of internal mobility and higher exchange protection, indicating stronger interaction, compared to the C-lobe, with the iNOS peptide. Taken together, these data indicate that the CaM-iNOS complex has increased internal mobility at lower Ca^{2+} concentrations, with a more dynamic C-lobe than N-lobe.

CaM is able to fine-tune the orientation of its domain and residue contacts to accommodate its binding to a variety of target proteins. The structures of CaM interacting with target peptides derived from the three enzymes have all been shown to be very similar, consisting of a globular lobe lined by a short connector wrapped around the helical peptide target. However, the three NOS enzymes show different Ca^{2+} dependent activation by CaM with the iNOS enzyme being fully active at basal levels of Ca^{2+} (<100 nM) in a cell, and the cNOS enzymes requiring 200-300 nM concentrations of free Ca^{2+} (54,55). Most investigations have focused on the Ca^{2+} dependent activation of NOS enzymes by CaM under non-physiological conditions such as in the presence of excess Ca^{2+} or excess Ca^{2+} chelator. The dynamics of the binding of CaM to the NOS enzymes analyzed using NMR H/D exchange and ^{15}N relaxation experiments performed at physiologically relevant free Ca^{2+} concentrations provide a better understanding of the physiologically relevant process.

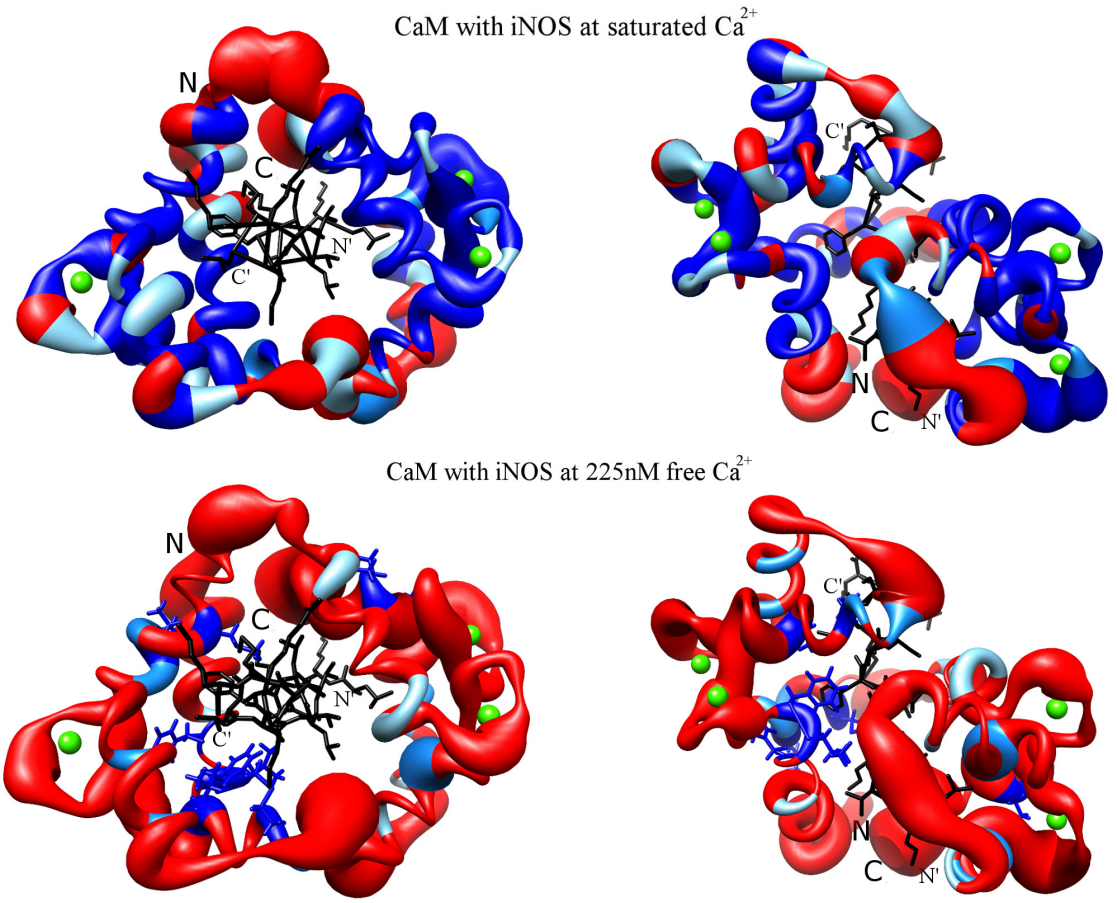

Figure 5. Worm models of CaM-iNOS peptide complexes at 225 nM Ca^{2+} and saturated Ca^{2+} illustrating their internal dynamics and amide H/D exchange data. The worm radius and H/D exchange rates are displayed the same as in Figure 3C and F. Worm models and amide H/D exchange data for CaM-iNOS complex at saturating Ca^{2+} and 225nM free Ca^{2+} concentrations were projected onto the previously determined structure of Ca^{2+}-replete CaM-iNOS (PDB 2LL6). The images were created using Chimera.

NMR H/D exchange and ^{15}N relaxation experiments show the CaM-iNOS and CaM-eNOS complexes exhibit similar dynamic differences between 225 nM and saturating Ca^{2+} concentrations; however, the individual CaM lobes interact differently with the two peptide at low Ca^{2+} concentrations. The increased internal dynamics and lower complex stability observed for CaM-iNOS and CaM-eNOS at low Ca^{2+} is further supported by previous binding kinetic experiments (68,70). These experiments showed at low Ca^{2+} concentrations CaM's binding affinity for eNOS and iNOS is decreased 4-fold and 5-fold, respectively, compared to saturated conditions due to decreased association rates and increased dissociation rates. These results also provide further evidence of the stronger interaction of the N-lobe of CaM with the iNOS peptide compared to with the eNOS peptide, contributing to the stronger binding of CaM with iNOS (65,71,72). In addition, this approach identified the roles played by the N and C lobes of CaM in the binding and activation of the NOS enzymes.

3.2. NOS-peptide interactions with apoCaM

CaM is able to bind to target proteins in the Ca^{2+}-replete and Ca^{2+}-deplete forms. At elevated Ca^{2+} concentrations, CaM binds to and activates eNOS making it a Ca^{2+}-dependent NOS enzyme. In contrast, iNOS is binds to CaM at basal levels of Ca^{2+} and is a Ca^{2+}-independent NOS enzyme (73–75). To study the Ca^{2+}-dependent/independent properties of binding and activation of iNOS by CaM, numerous studies use a series of CaM mutants. These include mutations of glutamate to glutamine residues at position 12 of each EF hand (76,77) or mutation of the conserved aspartate to alanine at position 1 of each EF hand (78–80). Changing the aspartate residue at position 1 of the EF hand loop of CaM inactivates the EF hand toward Ca^{2+} binding. These CaM proteins are defective in Ca^{2+} binding in either the N-terminal lobe EF hands (CaM_{12}; CaM D20A and D56A mutations), the C-terminal lobe EF hands (CaM_{34}; CaM D93A and D129A), or all four of its Ca^{2+}-binding EF hands (CaM_{1234}; mutations at D20A, D56A, D93A and D129A inclusive).

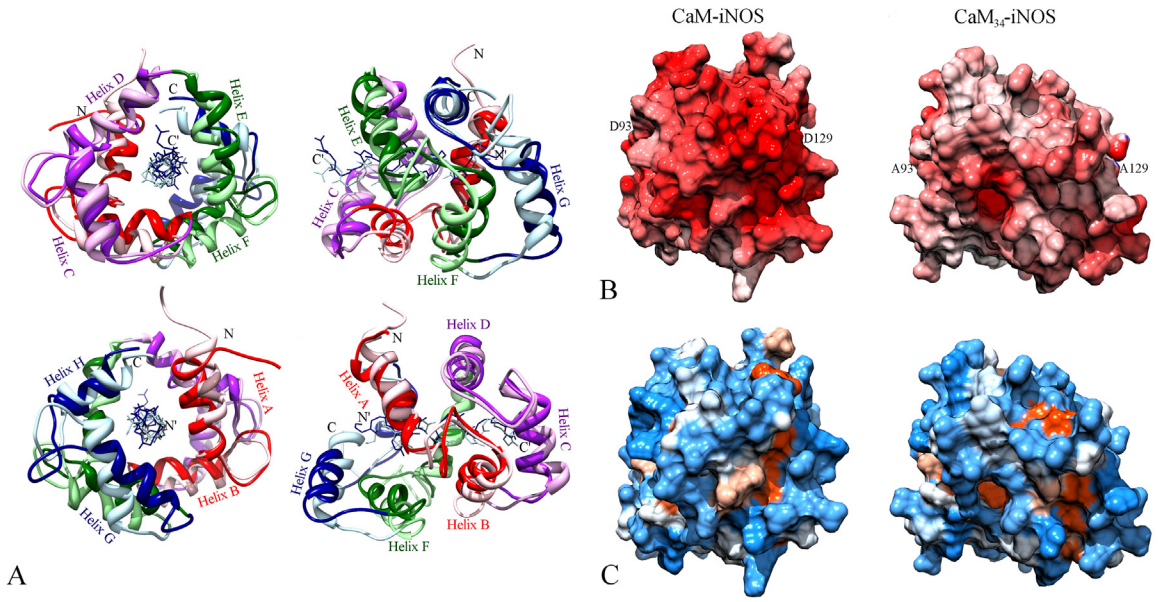

Figure 6. Comparison of the solution structure of the CaM_{34}-iNOS peptide complex (PDB 5TP5) with the solution structure of Ca^{2+}-replete CaM-iNOS peptide complex (PDB 2LL6). (A) The solution structures of the CaM_{34}-iNOS peptide (dark colors) and the Ca^{2+}-replete CaM-iNOS (light colors) are aligned by super- imposition of the backbone atoms of the N-lobes of CaM and the iNOS peptides viewed along the bound peptide from its C-terminus (C′) to its N-terminus (N′) in A and subsequently rotated 90° around the vertical axis in B. The superposition is viewed along the bound peptide from its N-terminus (N′) to its C-terminus (C′) in C and subsequently rotated 90° around the vertical axis in D. Calcium ions were omitted for clarity. The color scheme is the same as Figure 3. (B) Electrostatic potentials were calculated using the adaptive Poisson-Boltzmann solver (APBS) and PDB 2PQR software packages (107,108). The APBS-calculated electrostatic potential maps are projected on the surface of the C-lobes of the solution structure of the CaM-iNOS peptide complex and solution structure of the CaM_{34}-iNOS peptide complex. (C) The hydrophobicity surface calculated in Chimera, using the Kyte-Doolittle scale (109), projected onto the surface of the C-lobes of the solution structure of the CaM-iNOS peptide complex and solution structure of the CaM_{34}-iNOS peptide complex . The electrostatic potential maps are colored with a Chimera color key ranging from red (acidic, -10 kT/e) to blue (basic, 10 kT/e). The hydrophobicity surface is colored from blue (4.5.) for the most hydrophilic, to white, to orange red (−4.5.) for the most hydrophobic. The images were created using Chimera.

A previous study of iNOS activity using these CaM mutants to determine if the Ca^{2+}-free N- or C-lobe of CaM was responsible for the Ca^{2+}-independent association of CaM to iNOS found that iNOS was active for both CaM_{34} and CaM_{12}, with CaM_{34} NO· production rates similar to Ca^{2+}-replete CaM and CaM_{12} NO· production rates similar to apoCaM, in the presence of Ca^{2+}, whereas CaM_{1234} produced significantly reduced rates. In the presence of EDTA, wild type CaM and CaM_{34} showed a substantial decrease in iNOS activity, whereas no substantial decrease in iNOS activity was found for CaM_{12} or CaM_{1234} (81). The solution structure of CaM_{34} bound to the iNOS CaM binding domain peptide was determined because it was the only one to have differences in activation of iNOS in the presence and absence of Ca^{2+} and it was compared to the previously determined Ca^{2+}-replete CaM−iNOS complex to provide further insight into this decrease in activity (70). The solution structure of CaM_{1234} was also determined and the effects of these mutations were compared to the previous solution structure of apoCaM to determine the causes of CaM_{1234}'s lower activation with iNOS compared to apoCaM.

The CaM_{34}-iNOS complex has a Ca^{2+}-replete N-lobe and a Ca^{2+}-deplete C-lobe bound to the iNOS peptide (Figure 6). This structure shows CaM is still able to bind to iNOS with both lobes, even when the C-lobe of CaM is Ca^{2+}-deplete due to the Asp to Ala mutations. Comparison of the CaM_{34}-iNOS structure to the solution structure of Ca^{2+}-replete CaM-iNOS reveals similar N-lobes, whereas the Ca^{2+} binding loops of EF hands III and IV display differences between the structures. The mutation causes the Ca^{2+} binding loops of EF hands III and IV to adopt a less compact conformation in the CaM_{34}-iNOS structure. This causes local structural changes, such as the loop region connecting EF hands III and IV to move closer to the iNOS peptide, and long- range structural conformation changes, observed in the loop region connecting EF hands I and II and helix B. These loop regions contain multiple hydrophobic residues that pack close together and interact with the hydrophobic residues of the iNOS peptide. The EF hand Ca^{2+}-binding loops of the C-lobe of CaM_{34} have a Ca^{2+}-deplete conformation similar to apoCaM; however the overall conformation of the helix−loop−helix motifs is similar to the "open" conformation observed in the Ca^{2+}-replete form due to the interaction with the highly hydrophobic iNOS peptide. The mutations also cause a decrease in the electronegative surface potential of CaM's C-lobe, which may cause nonnative-like apoCaM interactions with other regions of the iNOS enzyme.

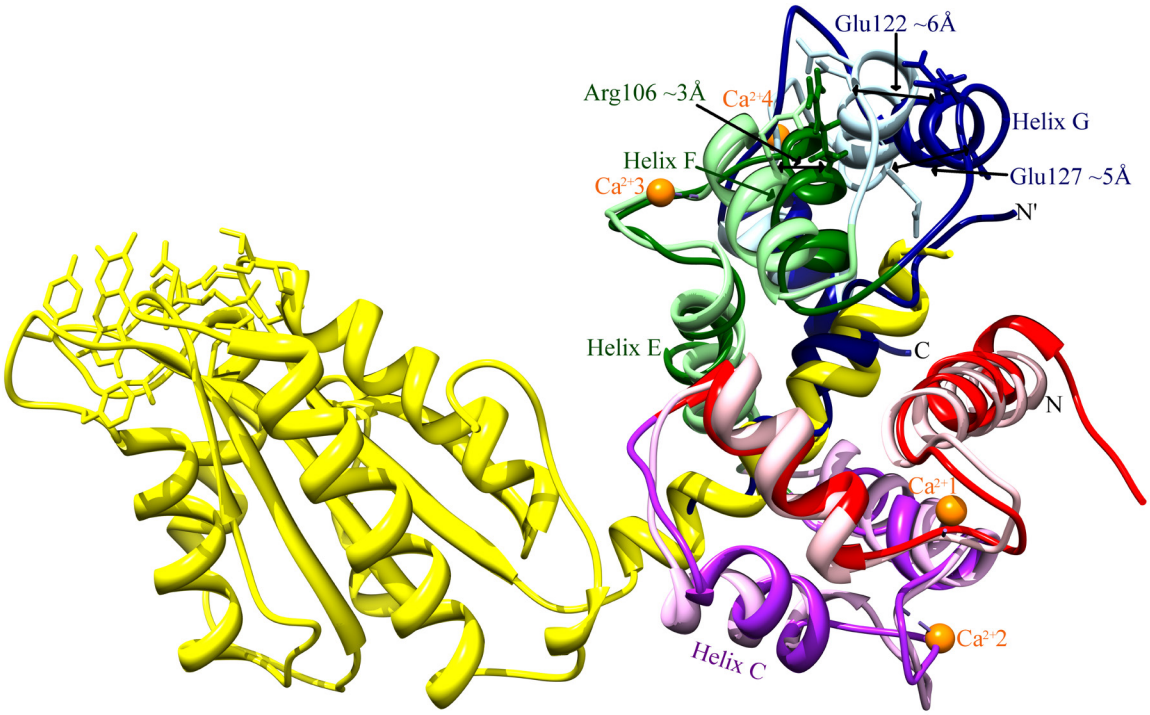

Figure 7. Solution structure of the CaM_{34}–iNOS peptide (dark colors, PDB 5TP6) and the crystal structure of the iNOS oxy-FMN-Ca^{2+}-replete CaM complex (CaM in light colors, iNOS CaM binding and FMN domains in yellow, PDB 3HR4) are aligned by superimposition of the backbone atoms of CaM and the iNOS CaM binding domain. The side chains of key residues of CaM that interact with iNOS' heme domains and the distance of their shifts are labeled. Residues 1−40 of CaM (EF hand I) are colored red, residues 41−79 (EF hand II) purple, residues 80−114 (EF hand III) green, and residues 115−148 (EF hand IV) blue. The peptide is colored lighter blue. Calcium ions are shown as orange spheres and labeled. Reprinted with permission from Biochemistry, 56, Piazza M, Taiakina V, Dieckmann T, Guillemette JG. Structural Consequences of Calmodulin EF Hand Mutations, 944–956, Copyright (2017) American Chemical Society. The images were created using Chimera.

For full activation of iNOS by CaM it has been shown that interaction of CaM with both the oxygenase and reductase domains of iNOS is required to stabilize the iNOS output state in addition to binding of CaM to iNOS' CaM binding domain (55,72,82). The interaction of CaM with iNOS is largely electrostatic, with the negative residues of CaM's N- and C-lobes interacting with the positive residues at the heme and FMN domain interfaces (71,83,84).

Some potential important connections required for full activity of iNOS are E47 of CaM with R536 of the FMN domain; D122 of CaM with R83 and R86 of the inter-monomer heme domain; and R106 of CaM with E285 of the intra-monomer heme domain. Molecular dynamics, X-ray crystallography, and electron cryo-microscopy studies showed that CaM undergoes conformational changes, along with the FMN and heme domains, from the input to the output state. During the movement of the FMN domain to the output state the shifting of the CaM binding domain causes the EF hand loops III and IV move by about 2 and 5 Å, respectively, while the N-lobe has a much larger conformational change, due to its interaction with the FMN domain (84). These interactions, are kept fully intact in the CaM_{34}–iNOS structure. The CaM_{34} mutation causes C-lobe of CaM to mimic the conformation of CaM interacting with the heme domain in the output state, specifically R106 of EF hand III moves about 3 Å and residues D122 and E127 of EF hand IV move about 6 and 5 Å, respectively (Figure 7). Meanwhile, helix E of the C-lobe of CaM_{34}, which is found to interact with the FMN domain, does not move relative to Ca^{2+}-replete CaM. The CaM_{34} mutation puts the C-lobe of CaM in a conformation that has interactions that stabilize the heme domain's output state conformation, and still allows the unmutated N-lobe of CaM to have the conformational movement with the FMN domain that is necessary to facilitate the inter domain electron transfer, which explains the full activity of iNOS in the presence of Ca^{2+}. The reduced iNOS activity observed for CaM_{34} in the presence of EDTA could be caused by the removal of Ca^{2+} from the N-lobe, leading to the rearrangement of EF hands I and II, which would affect the residues of helix C that interact with the FMN domain (Figure 7). Although CaM is still bound to the CaM binding domain of the enzyme due to strong hydrophobic interactions, this conformational change may not allow for the necessary interactions of the N-lobe of CaM to the FMN domain of iNOS required for efficient electron transfer. This may prevent the FMN conformational change required

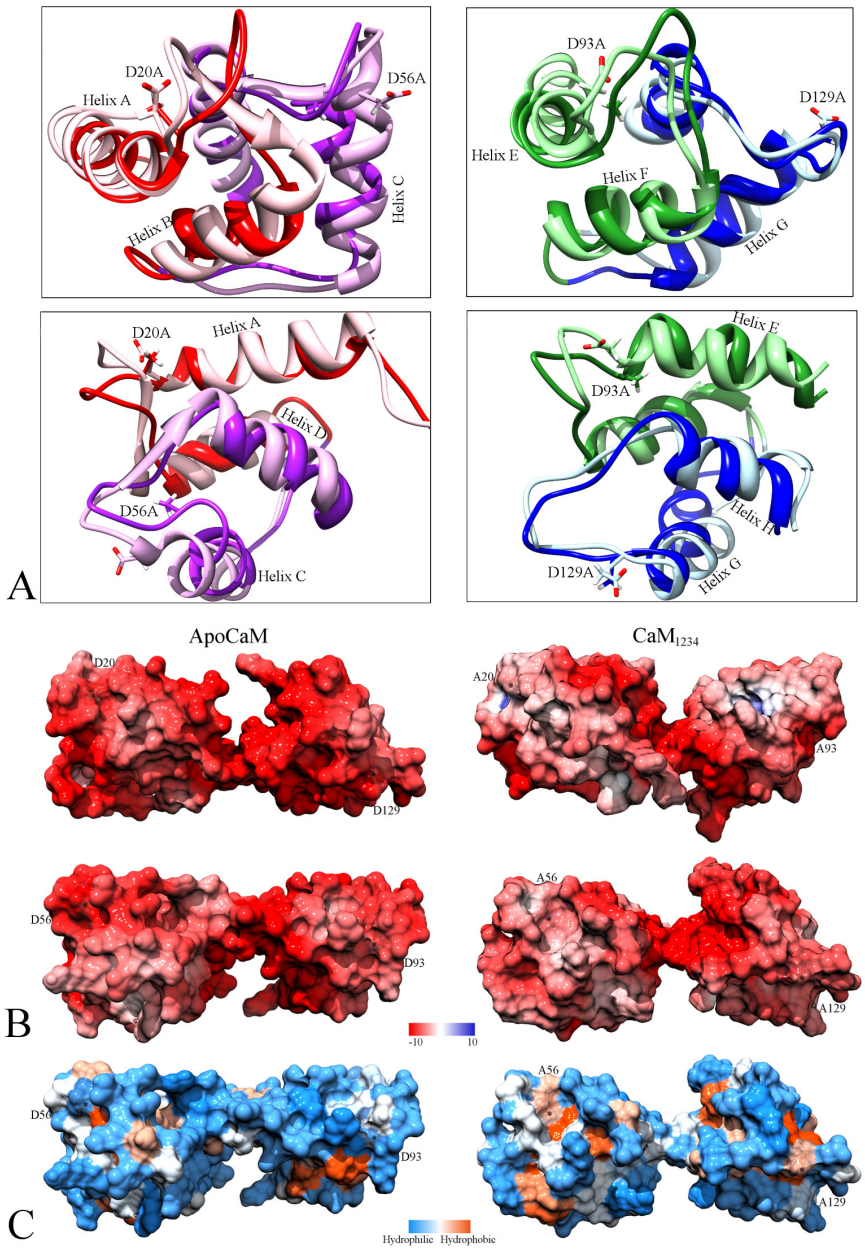

Figure 8. Comparison of the solution structure of the CaM_{1234} (PDB 5TP5) with the solution structure of apoCaM (PDB 1CFD). (A) The solution structures of CaM_{1234} (dark colors) and apoCaM (light colors, structure from PDB 1CFD (42)) are overlaid. For clarity only the N-lobes and the C-lobes of CaM_{1234} and apoCaM were superimposed separately. The side chains of Asp in apoCaM and Ala in CaM_{1234} are shown and labeled as D20A, D56A, D93A, and D129A. Residues 1−40 of CaM (EF hand I) are colored red, residues 41−79 (EF hand II) purple, residues 80−114 (EF hand III) green, and residues 115−148 (EF hand IV) blue. The peptide is colored lighter blue. (B) The APBS-calculated electrostatic potential maps projected on the surface of apoCaM (solution structure from PDB 1CFD (42)) and the CaM_{1234} solution structure. (C) The hydrophobicity surface calculated in chimera, using the Kyte-Doolittle scale, projected onto apoCaM and the CaM_{1234} solution structures. The electrostatic potential maps and hydrophobicity surfaces are colored as in Figure 6. The mutation sites D20A, D56A, D93A, and D129A are labeled and indicated by *. The images were created using Chimera.

for efficient electron transfer to the heme domain or prevent CaM from stabilizing the FMN to heme electron transfer in the output state (56,57,83,85).

The structural rationale for the lower activity observed for CaM_{1234} with iNOS can be explained by comparing the structure of apoCaM to CaM_{1234} (Figure 8). Although CaM_{1234} is still able to bind to the highly hydrophobic CaM-binding domain of iNOS, the structural perturbations and electrostatic surface potential changes induced by the EF hand mutations may affect how CaM_{1234} interacts with the rest of iNOS, specifically CaM's N-lobe interaction with the FMN domain. The less hydrophilic and less negative

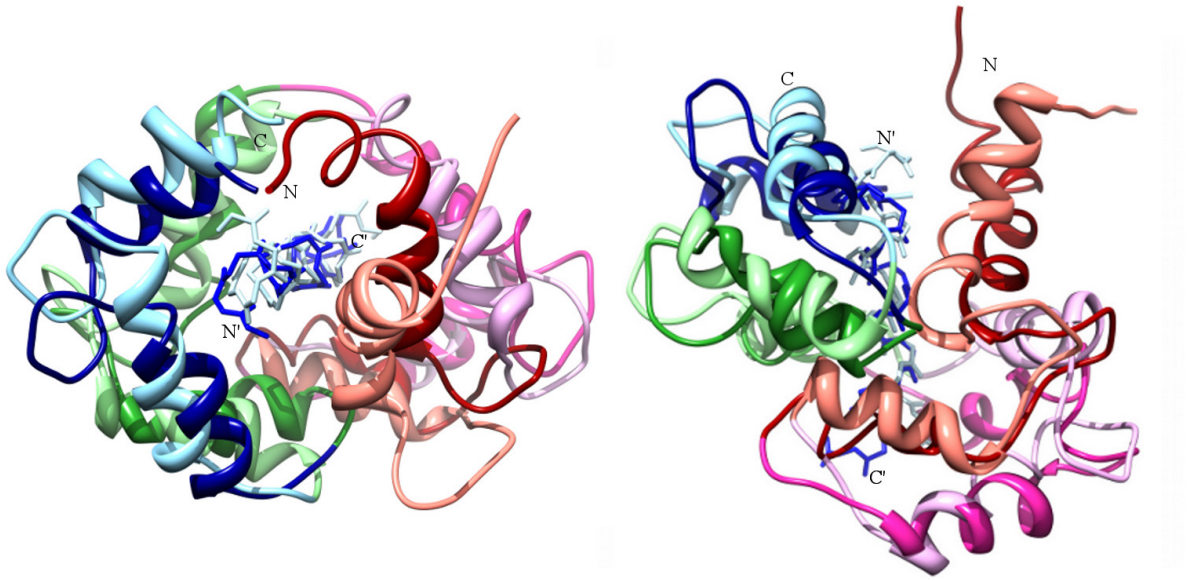

Figure 9. Superpositions of the CaM-eNOS peptide solution structure (PDB 2LL7) and the CaM-eNOSpThr495 peptide solution structure. Comparison of solution structures of CaM-eNOSpThr495 peptide (dark colors) with CaM-eNOS peptide (light colors) by superimposing the two structures and viewing it along the bound peptide from its N-terminus (N') to its C-terminus (C') on the left (front view), and rotated 90° around the horizontal axis with the N-terminus of the bound peptide on the top on the right (bottom view). The two structures are aligned by superimposing backbone atoms of the bound peptides. Residues 1−40 of CaM (EF hand I) are colored red, residues 41−79 (EF hand II) purple, residues 80−114 (EF hand III) green, and residues 115−148 (EF hand IV) blue. The peptide is colored lighter blue. Reprinted with permission from Biochemistry, 53, Piazza M, Taiakina V, Guillemette SR, Guillemette JG, Dieckmann T. Solution structure of calmodulin bound to the target peptide of endothelial nitric oxide synthase phosphorylated at thr495, 1241–1249, Copyright (2014) American Chemical Society. The images were created using Chimera.

electrostatic surface of CaM_{1234} would affect its interaction with the positive surface residues of iNOS at the CaM-FMN interface. This would prevent CaM from stabilizing the output state of the FMN and heme domains.

3.3. Phosphorylation modification of eNOS enzymes

The binding of CaM and the transfer of electrons from the reductase to the oxygenase domain of eNOS is regulated by multiple mechanisms, including protein phosphorylation and dephosphorylation (65,86). The eNOS enzyme contains many potential phosphorylation sites that can play a role in regulating its activity (87–90). For example, phosphorylation of S1177 in the reductase domain has been found to result in the activation of eNOS, whereas the phosphorylation of T495 within the CaM-binding domain has been found to act as a negative regulatory site reducing eNOS activity (91–93). A number of diseases have reported perturbations of eNOS phosphorylation (94). Phosphorylation of T495 has been reported to interfere with the binding of CaM to the CaM-binding domain affecting activation of the enzyme (86,91). The structural and functional effects that the phosphorylation of T495 in eNOS has on the Ca^{2+} dependent binding to CaM were investigated by the determination of the solution structure of CaM bound to the eNOS CaM-binding domain peptide phosphorylated at T495. This investigation was used to assess changes to the CaM-eNOS complex due to the phosphorylation of T495.

3.3.1. Comparison of the CaM-eNOS vs CaM-eNOSpThr495 complexes

Comparison of the CaM-eNOS and the CaM-eNOSpThr495 solution structures shows the two structures are quite similar, with a few local differences (Figure 9). The orientation of helix A of CaM is different between the two structures, with helix A of CaM-eNOSpThr495 pushed away from the N-terminus of the peptide (where the phosphorylated T495 is located). EF hand IV (colored blue) is also shifted farther away from the peptide in the CaM-eNOSpThr495 structure. The rest of the CaM-eNOSpThr495 structure confirms that the phosphorylation of T495 does not have an effect on the structure of CaM away from the site of the phosphorylation.

3.3.2. Electrostatic effects of the phosphorylation of T495

The EF hands I and IV are sensitive to the phosphorylation state at T495 of the eNOS peptide. The DelPhi analysis of the CaM-eNOSpThr495 structure (using the DelphiController interface of UCSF Chimera version 1.5.3. build 33475 (95)) shows this phosphorylation creates a more negative potential on

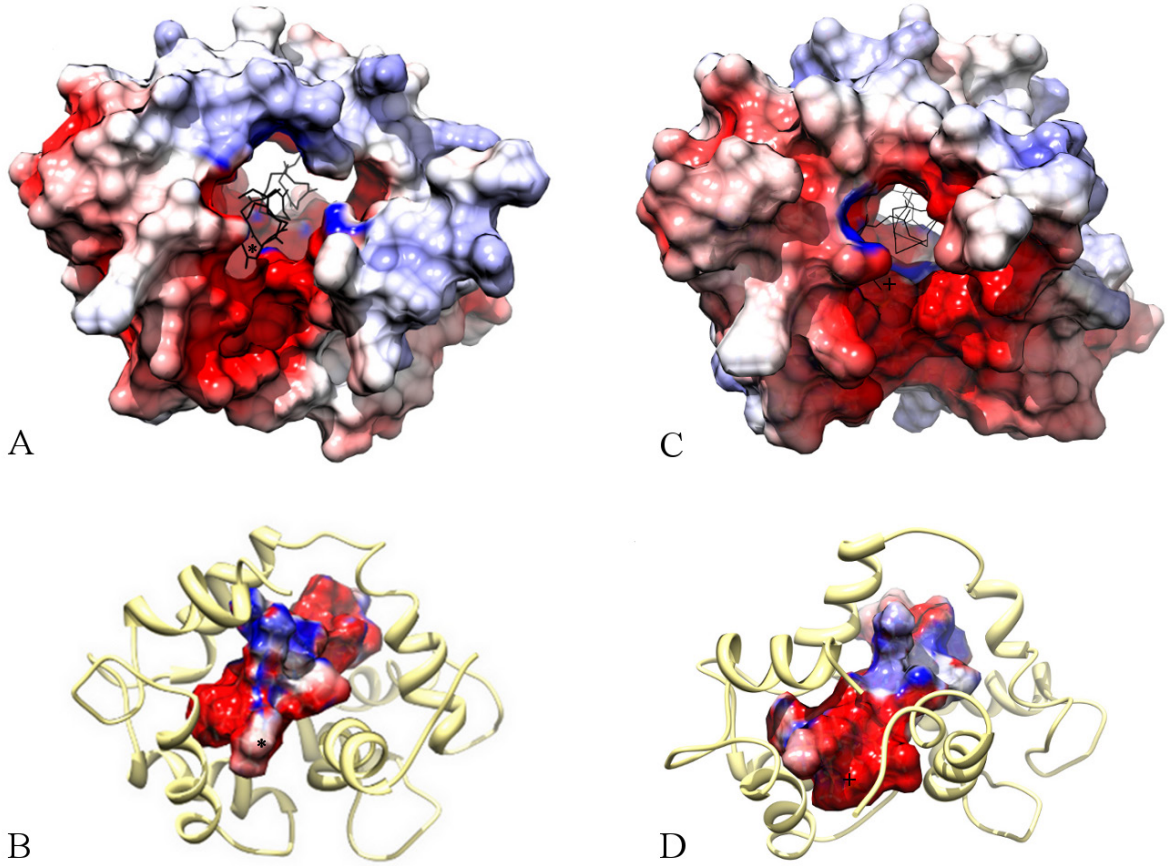

Figure 10. Delphi-calculated electrostatic potential maps. The Delphi-calculated electrostatic potential maps are projected on (A, B) the surface of the CaM-eNOS peptide complex (PDB 2LL7) and (C, D) the CaM-eNOSpThr495 peptide complex (PDB 2MG5). Thr495 and pThr495 are displayed on the peptide by an * and **+**. The Delphi-calculated electrostatic potential maps are colored with a Chimera color key ranging from (-15 kT/e) red to (15 kT/e) blue. Reprinted with permission from Biochemistry, 53, Piazza M, Taiakina V, Guillemette SR, Guillemette JG, Dieckmann T. Solution structure of calmodulin bound to the target peptide of endothelial nitric oxide synthase phosphorylated at thr495, 1241–1249, Copyright (2014) American Chemical Society. The images were created using Chimera.

the N-terminal region of the peptide, which is located in a negatively charged region of CaM and could lead to an electrostatic repulsion (Figure 10C, D). This negative charge is not present in the CaM-eNOS complex (Figure 10B) and thus would not cause any electrostatic repulsion. Residues E7, which is found in helix A of EF hand I, and E127, found in helix G of EF hand IV, of CaM are in close proximity to this phosphate group. An electrostatic repulsion between helix A of EF hand I and the phosphate group gives an explanation as to why helix A and helix G and EF hand IV are shifted further away from the eNOSpThr495 peptide in the CaM-eNOSpThr495 complex. This has been previously postulated by Aoyagi *et al*. when they suggested that the addition of a negatively charged phosphate group would cause electrostatic repulsion between E7 and E127 (96). This electrostatic repulsion could also be affecting CaM's ability to coordinate Ca^{2+} by interfering with the EF hands I and IV, which would help explain why at physiological Ca^{2+} levels CaM has a diminished ability to bind eNOS phosphorylated at T495.

Enzyme activity studies have shown that phosphorylation of T495 results in the loss of eNOS enzyme activity with the assumption being that phosphorylation of T495 hinders the association of CaM with its binding site on the eNOS enzyme (96). Until recently (64), there had not been a structural study using a phosphorylated T495 residue. Our solution structure shows that in the presence of excess Ca^{2+}, phosphorylation does not prevent the binding of CaM to the phosphorylated peptide; however, the phosphorylation prevents binding to CaM at lower Ca^{2+} concentrations that are similar to physiological Ca^{2+} levels. A comparison of the two structures show that the most significant changes in the CaM-eNOSpThr495 solution structure involved two CaM amino acids E7 and E127. In addition both E11 and M124 are found to be in close proximity to the pThr495 phosphate group. The Ca^{2+}-replete CaM-eNOS complex structure shows that the side chains of these amino acids are in contact with a number of amino acids in the eNOS peptide. The side chain of E7 is in contact with residue K497 of eNOS and has ionic interactions with R492,

while the side chain of E11 is in contact with residues A502 and I505 of eNOS and has a hydrogen bond with N501. The phosphorylation of T495 of eNOS introduces an electrostatic repulsion that pushes helix A (containing E7 and E11) away from the peptide likely disrupting the above mentioned interactions. The side chain of M124 is in contact with residues T495, F496 and V499 of eNOS, while residue E127 of CaM has contact with T495 and K497 and has ionic interactions with K493 and the backbone of T496. Electrostatic repulsion could again account for the displacement of helix G of EF hand 4 (containing M124 and E127) away from the peptide likely disrupting these interactions. The displacement of helix A and G may not be significant under conditions with 1 mM Ca^{2+}, but under physiological low Ca^{2+} concentration conditions, a larger relative displacement of these helices may have a detrimental effect on enzyme binding and activation. Affinity measurements using dansyl-labeled CaM experiments previously showed that the pThr495 peptide required significantly higher than physiological concentrations of Ca^{2+} to bind to CaM (64).

In summary, at saturating Ca^{2+} concentrations, the interactions of CaM with the peptides of the eNOS CaM binding domain or the eNOS CAM binding domain phosphorylated at T495 are very similar. At the lower Ca^{2+} concentration of 225 nM, near physiological Ca^{2+} levels, no significant binding of CaM to eNOSpThr495 is observed, whereas CaM binds to the wild type eNOS peptide. When T495 is phosphorylated, our results indicate there is an electrostatic repulsion that affects binding to CaM and may account for the diminished CaM-dependent activation of the eNOS enzyme under low physiological Ca^{2+} concentrations.

4. NMR METHODS FOR STUDYING LARGE PROTEINS

Currently, there is no NMR structural data of CaM interacting with the holo-NOS isoforms. As previously mentioned, since the complex of CaM with nNOS is extremely large (greater than 300 kDa for the dimer complex), conventional ^{1}H-^{15}N HSQC experiments have not been able to produce useful spectra. The impediment imposed by the large molecular weight of a CaM-NOS complex may be further complicated by the possibility that chemical exchange may also be present due to each NOS subunit experiencing different environments. While the large size of NOS enzymes is a significant challenge for NMR spectroscopy similar sized proteins have been investigated using transverse relaxation-optimized NMR spectroscopy (TROSY) (97–99). TROSY is only one advance in NMR spectroscopy that has opened up new explorations of large proteins and protein complexes. The TROSY experiment allows for higher sensitivity, narrow lines and a spectrum similar to an HSQC. Preliminary ^{15}N TROSY experiments in our lab have shown that structural data may be possible with this method, but will require large quantities of pure NOS enzyme and higher NMR field strength.

As outlined in a recent review article, advances in NMR spectroscopy provide new avenues for the study of structure and dynamics of large biomolecules (100). In the case of NOS enzymes, either the CaM or the truncated NOS isozymes can be selectively labeled for NMR studies (101) thus simplifying the assignment of peaks and allowing for the investigation of larger segments of the enzymes. NMR peak assignments can be based on published CaM resonance assignments using standard NMR triple resonance techniques. To monitor structural changes in the enzyme itself, NMR investigations can be performed on complexes with labeled CaM or NOS constructs containing ($\varepsilon^{13}C$)-labelled methionine. This would allow us to determine which residues of CaM interact with regions of the holoNOS enzymes other than the CaM-binding domains through chemical shift changes between the CaM-NOS peptides and CaM-holoNOS spectra. Chemical shift perturbations using methionine-TROSY spectra can provide information about interaction between the different NOS domains and CaM (102,103). Methionine methyl groups tend to resonate in largely unpopulated region of the (^{1}H,^{13}C) correlation spectrum making it a useful probe for protein dynamics (104). Methionine is a relatively rare residue making up approximately 2% of the total residues of each NOS isozyme. Naturally occurring Met residues are found in key regions and control elements found in all three NOS enzymes. This approach can be used to probe key regions and subdomains in each of the NOS isozymes. Because signals are not observed for the unlabeled residues of the complex, this approach simplifies the NMR spectra while still providing details of Met residues in key regions of the enzyme. The labeled NOS proteins can be generated by expression of the recombinant gene in an *E. coli* methionine auxotroph supplemented with (ε ^{13}C)-labelled methionine (105). A systematic approach can be used combining our knowledge of the structure and select methionine replacements to identify key residues in important regions of the enzymes and probe for structural changes in NOS in the absence and presence of CaM and Ca^{2+}.

A further complication comes from cryo EM studies showing that only one of the FMNs at a time in the dimer transfers electrons inter-molecularly to the heme (56,58,61) . This process could result in mixed signals form the FMN subdomains experiencing different environments. To overcome this problem, mixed dimers could be generated to simplify the assignment of structural and dynamic interactions. Mixed dimers could be produced by the co-expression in *E. coli* of truncated constructs (i.e. Oxy-CaM and labeled Oxy-FMN or holoenzyme) with two

different affinity tagged versions of the NOS subunits allowing for the purification of mixed dimers in two chromatography steps (106). In concert with the use of mixed dimers, the method to “label, express, and generate oligomers” for NMR (LEGO-NMR) could be performed in *E. coli* cells. This method utilizes two plasmids carrying different promoters so that only the monomer containing the FMN domain is expressed in an NMR active medium whereas a second monomer (Oxy-CaM) can be produced in an NMR invisible medium (101). This approach could be used to investigate key isoform specific structural and functional features of the output state.

5. ACKNOWLEDGMENT

Molecular graphics images were produced using the UCSF Chimera package from the Resource for Biocomputing, Visualization, and Informatics at the University of California, San Francisco. The authors declare that the research was conducted in the absence of any commercial or financial relationships that could be construed as a potential conflict of interest. All authors participated in the drafting, writing and approval of the final version of this review.This work was supported, in whole or in part, by the Natural Sciences and Engineering Research Council of Canada (NSERC) via Grants 326911 (to T.D) and 183521 (to J.G.G).

6. REFERENCES

1. K. Wüthrich: *NMR of proteins and nucleic acids*. Wiley Toronto, Ontario, Canada (1986)

2. A.K. Mittermaier, L.E. Kay: New Tools Provide New Insights in NMR Studies of Protein Dynamics. *Science* 312, 224–228 (2006)
DOI: 10.1126/science.1124964

3. J. Cavanagh, W. J. Fairbrother, A. G. I. Palmer, M. Rance, N. J. Skelton: *Protein NMR Spectroscopy: Principles and Practice*. Second Edi. Elsevier Academic Press San Diego, California (2007)

4. A. G. Tzakos, C. R. R. Grace, P. J. Lukavsky, R. Riek: NMR techniques for very large proteins and RNAs in solution. *Annu Rev Biophys Biomol Struct* 35, 319–342 (2006)
DOI: 10.1146/annurev.biophys.35.040405.102034

5. V. Tugarinov, V Kanelis, L. E. Kay: Isotope labeling strategies for the study of high-molecular-weight proteins by solution NMR spectroscopy. *Nat Protoc* 1, 749–754 (2006)
DOI: 10.1038/nprot.2006.101

6. L. E. Kay: NMR studies of protein structure and dynamics. *J Magn Reson* 173, 193–207 (2005)
DOI: 10.1016/j.jmr.2004.11.021

7. T. L. James, N. K. Oppenheimer: *Methods in Enzymology. Volume 239. Nuclear Magnetic Resonance Part C.* Academic Press San Diego, California (1994)

8. D. Neuhaus, M. P. Williamson: *The Nuclear Overhauser Effect in Structural and Conformational Analysis*. Second. Wiley New York, New York (2000)

9. J. N. S. Evans: *Biomolecular NMR spectroscopy*. Oxford University Press Inc. New York, New York (1995)

10. R. Ernst, G. Bodenhausen, A. Wokaun: *Principles of nuclear magnetic resonance in one and two dimensions*. Oxford University Press Inc. New York, New York (1987)

11. G. M. Clore, A. M. Gronenborn: Structures of larger proteins in solution: three- and four-dimensional heteronuclear NMR spectroscopy. *Science* 252, 1390–1399 (1991)
DOI: 10.1126/science.2047852

12. G. Bodenhausen, D. J. Ruben: Natural abundance nitrogen-15 NMR by enhanced heteronuclear spectroscopy. *Chem Phys Lett* 69 185–189 (1980)
DOI: 10.1016/0009-2614(80)80041-8

13. L. E. Kay, M. Ikura, R. Tschudin, A. Bax: Three-dimensional triple-resonance NMR spectroscopy of isotopically enriched proteins. *J Magn Reson* 89, 496–514 (1990)
DOI: 10.1016/0022-2364(90)90333-5

14. S. Grzesiek, A. Bax: Correlating backbone amide and side chain resonances in larger proteins by multiple relayed triple resonance NMR. *J Am Chem Soc* 114, 6291–6293 (1992)
DOI: 10.1021/ja00042a003

15. A. Bax, M. Ikura: An efficient 3D NMR technique for correlating the proton and ^{15}N backbone amide resonances with the α-carbon of the preceding residue in

uniformly $^{15}N/^{13}C$ enriched proteins. *J Biomol NMR* 1, 99–104 (1991)
DOI: 10.1007/BF01874573

16. A. Bax, M. Clore, A. M. Gronenborn: ^{1}H-^{1}H Correlation via Isotropic Mixing of ^{13}C a New Three-Dimensional Approach for Assigning ^{l}H and ^{13}C Spectra of ^{13}C-Enriched Proteins. *J Magn Reson* 88, 425–431 (1990)

17. A. H. Kwan, M. Mobli, P. R. Gooley, G. F. King, J. P. Mackay: Macromolecular NMR spectroscopy for the non-spectroscopist. *FEBS J* 278, 687–703 (2011)
DOI: 10.1111/j.1742-4658.2011.08004.x

18. R. Ishima, D. A. Torchia: Protein dynamics from NMR. *Nat Struct Biol* 7, 740–743 (2000)
DOI: 10.1038/78963

19. L. E. Kay: Protein dynamics from NMR. *Biochem Cell Biol* 76, 145–152 (1998)
DOI: 10.1139/o98-024

20. J. G. Kempf, J. P. Loria: Protein dynamics from solution NMR: theory and applications. *Cell Biochem Biophys* 37, 187–211 (2003)
DOI: 10.1385/CBB:37:3:187

21. A. J. Wand: Dynamic activation of protein function: a view emerging from NMR spectroscopy. *Nat Struct Biol* 8, 926–931 (2001)
DOI: 10.1038/nsb1101-926

22. T. C. Pochapsky, S. Kazanis, M. Dang: Conformational plasticity and structure/function relationships in cytochromes P450. *Antioxid Redox Signal* 13, 1273–1296 (2010)
DOI: 10.1089/ars.2010.3109

23. K. Sikic, S. Tomic, O. Carugo: Systematic comparison of crystal and NMR protein structures deposited in the protein data bank. *Open Biochem J* 4, 83–95 (2010)
DOI: 10.2174/1874091X01004010083

24. G. M. Clore, J. Iwahara: Theory, practice, and applications of paramagnetic relaxation enhancement for the characterization of transient low-population states of biological macromolecules and their complexes. *Chem Rev* 109, 4108–4139 (2009)
DOI: 10.1021/cr900033p

25. G. M. Clore: Exploring sparsely populated states of macromolecules by diamagnetic and paramagnetic NMR relaxation. *Protein Sci* 20, 229–246 (2011)
DOI: 10.1002/pro.576

26. B. Ma, R. Nussinov: Polymorphic triple beta-sheet structures contribute to amide hydrogen/deuterium (H/D) exchange protection in the Alzheimer amyloid beta42 peptide. *J Biol Chem* 286, 34244–34253 (2011)
DOI: 10.1074/jbc.M111.241141

27. M. Andrec, R. B. Hill, J. H. Prestegard: Amide exchange rates in Escherichia coli acyl carrier protein: correlation with protein structure and dynamics. *Protein Sci* 4, 983–993 (1995)
DOI: 10.1002/pro.5560040518

28. V. I. Polshakov, B. Birdsall, J. Feeney: Effects of co-operative ligand binding on protein amide NH hydrogen exchange. *J Mol Biol* 356, 886–903 (2006)
DOI: 10.1016/j.jmb.2005.11.084

29. M. M. G. Krishna, L. Hoang, Y. Lin, S. W. Englander: Hydrogen exchange methods to study protein folding. *Methods* 34, 51–64 (2004)
DOI: 10.1016/j.ymeth.2004.03.005

30. I. A. Kaltashov, C. E. Bobst, R. R. Abzalimov: H/D exchange and mass spectrometry in the studies of protein conformation and dynamics: Is there a need for a top-down approach? *Anal Chem* 81, 7892–7899 (2009)
DOI: 10.1021/ac901366n

31. S. W. Englander, L. Mayne: Using Hydrogen-Exchange Labeling And Two - Dimensional Nmr. *Annu Rev Biophys Biomol Struct* 21, 243–265 (1992)
DOI: 10.1146/annurev.bb.21.060192.001331

32. S. W. Englander, N. Kallenbach: Hydrogen exchange and structural dynamics of proteins and nucleic acids. *Q Rev Biophys* 16, 521–655 (1983)
DOI: 10.1017/S0033583500005217

33. D. H. Williams, E. Stephens, D. P. O'Brien, M. Zhou: Understanding noncovalent interactions: ligand binding energy and catalytic efficiency from ligand-induced reductions in motion within receptors and enzymes. *Angew Chem Int Ed Engl* 43, 6596–6616 (2004)
DOI: 10.1002/anie.200300644

34. D. H. Williams, E. Stephens, M. Zhou: Ligand Binding Energy and Catalytic Efficiency from Improved Packing within Receptors and Enzymes. *J Mol Biol* 329, 389–399 (2003)
DOI: 10.1016/S0022-2836(03)00428-5

35. G. Lipari, A. Szabo: Model-free approach to the interpretation of nuclear magnetic resonance relaxation in macromolecules. 1. Theory and range of validity. *J Am Chem Soc* 104, 4546–4559 (1982)
DOI: 10.1021/ja00381a009

36. L. E. Kay, D. A. Torchia, A. Bax: Backbone Dynamics of Proteins as Studied by ^{15}N Inverse Detected Heteranuckar. *Biochemistry* 28, 8972–8979 (1989)
DOI: 10.1021/bi00449a003

37. L. E. Kay: New Views of Functionally Dynamic Proteins by Solution NMR Spectroscopy. *J Mol Biol* 428, 323–331 (2015)
DOI: 10.1016/j.jmb.2015.11.028

38. L. E. Kay, L. Frydman: A special "JMR Perspectives" issue: Foresights in biomolecular solution-state NMR spectroscopy - from spin gymnastics to structure and dynamics. *J Magn Reson* 241, 1–2 (2014)
DOI: 10.1016/j.jmr.2014.01.010

39. M. Ikura, J. B, Ames: Genetic polymorphism and protein conformational plasticity in the calmodulin superfamily: two ways to promote multifunctionality. *Proc Natl Acad Sci U S A* 103, 1159–1164 (2006)
DOI: 10.1073/pnas.0508640103

40. N. C. J. Strynadka, M. N. G. James: Crystal structures of the helix-loop-helix calcium-binding proteins. *Annu Rev Biochem* 58, 951–998 (1989)
DOI: 10.1146/annurev.bi.58.070189.004511

41. M. Zhang, T. Tanaka, M. Ikura: Calcium-induced conformational transition revealed by the solution structure of apo calmodulin. *Nat Struct Biol* 2, 758–767 (1995)
DOI: 10.1038/nsb0995-758

42. H. Kuboniwa, N. Tjandra, S. Grzesiek, H. Ren, C. B. Klee, A. Bax: Solution structure of calcium-free calmodulin. *Nat Struct Biol* 2, 768–776 (1995)
DOI: 10.1038/nsb0995-768

43. Y. S. Babu, C. E. Bugg, W. J. Cook: Structure of calmodulin refined at 2.2. A resolution. *J Mol Biol* 204, 191–204 (1988)
DOI: 10.1016/0022-2836(88)90608-0

44. S. Linse, A. Helmersson, S. Forsen: Calcium binding to calmodulin and its globular domains. *J Biol Chem* 266, 8050–8054 (1991)

45. S. Pedigo, M. A. Shea: Discontinuous equilibrium titrations of cooperative calcium binding to calmodulin monitored by 1D ^{1}H-nuclear magnetic resonance spectroscopy. *Biochemistry* 34, 10676–10689 (1995)
DOI: 10.1021/bi00033a044

46. W. K. Alderton, C. E. Cooper, R. G. Knowles: Nitric oxide synthases: structure, function and inhibition. *Biochem J* 357, 593–615 (2001)
DOI: 10.1042/bj3570593

47. S. Daff: NO synthase: structures and mechanisms. *Nitric Oxide* 23, 1–11 (2010)
DOI: 10.1016/j.niox.2010.03.001

48. A. R. Rhoads, F. Friedberg: Sequence motifs for calmodulin recognition. *FASEB J* 11, 331–340 (1997)

49. D. E. Spratt, V. Taiakina, M. Palmer, J. G. Guillemette: Differential binding of calmodulin domains to constitutive and inducible nitric oxide synthase enzymes. *Biochemistry* 46, 8288–8300 (2007)
DOI: 10.1021/bi062130b

50. R. Busse, A. Mulsch: Calcium-dependent nitric oxide synthesis in endothelial cytosol is mediated by calmodulin. *FEBS Lett* 265, 133–136 (1990)
DOI: 10.1016/0014-5793(90)80902-U

51. J-L. Balligand, D. Ungureanu-Longrois, W. W. Simmons, D. Pimental, T. A. Malinski, M. Kapturczak, Z. Taha, C. J. Lowenstein, A. J. Davidoff, R. A. Kelly, T. W. Smith, T. Michel: Cytokine-inducible nitric oxide synthase (iNOS) expression in cardiac myocytes. Characterization and regulation of iNOS expression and detection of iNOS activity in single cardiac myocytes *in vitro*. *J Biol Chem* 269, 27580–27588 (1994)

52. E. Carafoli: Intracellular calcium homeostasis. *Annu Rev Biochem* 56, 395–433 (1987)
DOI: 10.1146/annurev.bi.56.070187.002143

53. S. Islam: *Calcium Signaling*. Spinger New York, New York (2012)
DOI: 10.1007/978-94-007-2888-2

54. W. C. Sessa, J. K. Harrison, C. M. Barber, D. Zeng, M. E. Durieux, D. D. D. Angelo, K. R. Lynch, M. J. Peach: Molecular cloning and expression of a cDNA encoding endothelial

cell nitric oxide synthase. *J Biol Chem* 267, 15274–15276 (1992)

55. J. Ruan, Q. W. Xie, N. Hutchinson, H. Cho, G. C. Wolfe, C. Nathan: Inducible nitric oxide synthase requires both the canonical calmodulin-binding domain and additional sequences in order to bind calmodulin and produce nitric oxide in the absence of free Ca^{2+}. *J Biol Chem* 271, 22679–22686 (1996) DOI: 10.1074/jbc.271.37.22679

56. N. G. H. Leferink, S. Hay, S. E. J. Rigby, N. S. Scrutton: Towards the free energy landscape for catalysis in mammalian nitric oxide synthases. *FEBS J* 282, 3016–3029 (2014) DOI: 10.1111/febs.13171

57. A. Sobolewska-Stawiarz, N. G. H. Leferink, K. Fisher, D. J. Heyes, S. Hay, S. E. J. Rigby, N. S. Scrutton: Energy landscapes and catalysis in nitric-oxide synthase. *J Biol Chem* 289, 11725–11738 (2014) DOI: 10.1074/jbc.M114.548834

58. M. G. Campbell, B. C. Smith, C. S. Potter, B. Carragher, M. A. Marletta: Molecular architecture of mammalian nitric oxide synthases. *Proc Natl Acad Sci U S A* 111, E3614-3623 (2014) DOI: 10.1073/pnas.1413763111

59. Y. He, M. M. Haque, D. J. Stuehr, H. P. Lu: Single-molecule spectroscopy reveals how calmodulin activates NO synthase by controlling its conformational fluctuation dynamics. *Proc Natl Acad Sci U S A* 112, 11835–11840 (2015) DOI: 10.1073/pnas.1508829112

60. D. C. Arnett, A. Persechini, Q. K. Tran, D. J. Black, C. K. Johnson: Fluorescence quenching studies of structure and dynamics in calmodulin-eNOS complexes. *FEBS Lett* 589, 1173–1178 (2015) DOI: 10.1016/j.febslet.2015.03.035

61. N. Volkmann, P. Martásek, L. J. Roman, X-P. Xu, C. Page, M. Swift, D. Hanein, B. S. Masters: Holoenzyme structures of endothelial nitric oxide synthase - an allosteric role for calmodulin in pivoting the FMN domain for electron transfer. *J Struct Biol* 188, 46–54 (2014) DOI: 10.1016/j.jsb.2014.08.006

62. J. Tejero, M. M. Haque, D. Durra, D. J. Stuehr: A bridging interaction allows calmodulin to activate NO synthase through a bi-modal mechanism. *J Biol Chem* 285, 25941–25949 (2010) DOI: 10.1074/jbc.M110.126797

63. M. Matsubara, N. Hayashi, K. Titani, H. Taniguchi: Circular dichroism and ^{1}H NMR studies on the structures of peptides derived from the calmodulin-binding domains of inducible and endothelial nitric-oxide synthase in solution and in complex with calmodulin. *J Biol Chem* 272, 23050–23056 (1997) DOI: 10.1074/jbc.272.37.23050

64. M. Piazza, V. Taiakina, S. R. Guillemette, J. G. Guillemette, T. Dieckmann: Solution structure of calmodulin bound to the target Peptide of endothelial nitric oxide synthase phosphorylated at thr495. *Biochemistry* 53, 1241–1249 (2014) DOI: 10.1021/bi401466s

65. M. Piazza, K. Futrega, D. E. Spratt, T. Dieckmann, J. G. Guillemette: Structure and dynamics of calmodulin (CaM) bound to nitric oxide synthase peptides: Effects of a phosphomimetic caM mutation. *Biochemistry* 51, 3651–3661 (2012) DOI: 10.1021/bi300327z

66. M. Zhang, H. J. Vogel: Characterization of the calmodulin-binding domain of rat cerebellar nitric oxide synthase. *J Biol Chem* 269, 981–985 (1994)

67. M. Zhang, T. Yuan, J. M. Aramini, H. J. Vogel: Interaction of calmodulin with its binding domain of rat cerebellar nitric oxide synthase: A multinuclear NMR study. *J Biol Chem* 270, 20901–20907 (1995) DOI: 10.1074/jbc.270.36.20901

68. M. Piazza, J. G. Guillemette, T. Dieckmann: Dynamics of nitric oxide synthase–calmodulin interactions at physiological calcium concentrations. *Biochemistry* 54, 1989–2000 (2015) DOI: 10.1021/bi501353s

69. M. Piazza, T. Dieckmann, J. G. Guillemette: Structural Studies of a Complex Between Endothelial Nitric Oxide Synthase and Calmodulin at Physiological Calcium Concentration. *Biochemistry* 55, 5962–5971 (2016) DOI: 10.1021/acs.biochem.6b00821

70. M. Piazza, V. Taiakina, T. Dieckmann, J. G. Guillemette: Structural Consequences

of Calmodulin EF Hand Mutations. *Biochemistry* 56, 944–956 (2017)
DOI: 10.1021/acs.biochem.6b01296

71. C. Xia, I. Misra, T. Iyanagi, J-J. P. Kim: Regulation of interdomain interactions by calmodulin in inducible nitric-oxide synthase. *J Biol Chem* 284, 30708–30717 (2009)
DOI: 10.1074/jbc.M109.031682

72. R. C. Venema, H. S. Sayegh, J. D. Kent, D. G. Harrison: Identification, characterization, and comparison of the calmodulin-binding domains of the endothelial and inducible nitric oxide synthases. *J Biol Chem* 271, 6435–6440 (1996)
DOI: 10.1074/jbc.271.11.6435

73. H. J. Cho, Q. W. Xie, J. Calaycay, R. A. Mumford, K. M. Swiderek, T. D. Lee, C. Nathan: Calmodulin is a subunit of nitric oxide synthase from macrophages. *J Exp Med* 176, 599–604 (1992)
DOI: 10.1084/jem.176.2.599

74. Q. W. Xie, H. J. Cho, J. Calacay, R. A. Mumford, K. M. Swiderek, T. D. Lee, A. Ding, T. Troso, C. Nathan: Cloning and characterization of inducible nitric oxide synthase from mouse macrophages. *Science* 256, 225–228 (1992)
DOI: 10.1126/science.1373522

75. J. L. Urbauer, J. H. Short, L. K. Dow, A. J. Wand: Structural analysis of a novel interaction by calmodulin: high-affinity binding of a peptide in the absence of calcium. *Biochemistry* 34, 8099–8109 (1995)
DOI: 10.1021/bi00025a016

76. J. Evenäs, S. Forsén, A. Malmendal, M. Akke: Backbone dynamics and energetics of a calmodulin domain mutant exchanging between closed and open conformations. *J Mol Biol* 289, 603–617 (1999)
DOI: 10.1006/jmbi.1999.2770

77. J. F. Maune, C. B. Klee, K. Beckingham: Ca^{2+} binding and conformational change in two series of point mutations to the individual Ca^{2+}-binding sites of calmodulin. *J Biol Chem* 267, 5286–5295 (1992)

78. J. R. Geiser, D. van Tuinen, S. E. Brockerhoff, M. M. Neff, T. N. Davis: Can calmodulin function without binding calcium? *Cell* 65, 949–959 (1991)
DOI: 10.1016/0092-8674(91)90547-C

79. X. M. Xia, B. Fakler, A. Rivard, G. Wayman, T. Johnson-Pais, J. E. Keen, T. Ishii, B. Hirschberg, C. T. Bond, S. Lutsenko, J. Maylie, J. P. Adelman: Mechanism of calcium gating in small-conductance calcium-activated potassium channels. *Nature* 395, 503–507 (1998)
DOI: 10.1038/26758

80. L-W. Xiong, Q. K. Kleerekoper, X. Wang, J. A. Putkey: Intra- and interdomain effects due to mutation of calcium-binding sites in calmodulin. *J Biol Chem* 285, 8094–8103 (2010)
DOI: 10.1074/jbc.M109.065243

81. D. E. Spratt, V. Taiakina, J. G. Guillemette: Calcium-deficient calmodulin binding and activation of neuronal and inducible nitric oxide synthases. *Biochim Biophys Acta* 1774, 1351–1358 (2007)
DOI: 10.1016/j.bbapap.2007.07.019

82. S. J. Lee, J. T. Stull: Calmodulin-dependent regulation of inducible and neuronal nitric-oxide synthase. *J Biol Chem* 273, 27430–27437 (1998)
DOI: 10.1074/jbc.273.42.27430

83. B. C. Smith, E. S. Underbakke, D. W. Kulp, W. R. Schief, M. A. Marletta: Nitric oxide synthase domain interfaces regulate electron transfer and calmodulin activation. *Proc Natl Acad Sci U S A* 110, E3577–E3586 (2013)
DOI: 10.1073/pnas.1313331110

84. Y. Sheng, L. Zhong, D. Guo, G. Lau, C. Feng: Insight into structural rearrangements and interdomain interactions related to electron transfer between flavin mononucleotide and heme in nitric oxide synthase: A molecular dynamics study. *J Inorg Biochem* 153, 186–196 (2015)
DOI: 10.1016/j.jinorgbio.2015.08.006

85. S. A. Hollingsworth, J. K. Holden, H. Li, T. L. Poulos: Elucidating nitric oxide synthase domain interactions by molecular dynamics. *Protein Sci* 25, 374–382 (2016)
DOI: 10.1002/pro.2824

86. I. Fleming, R. Busse: Molecular mechanisms involved in the regulation of the endothelial nitric oxide synthase. *Am J Physiol Regul Integr Comp Physiol* 284, R1-12 (2003)
DOI: 10.1152/ajpregu.00323.2002

87. I. Fleming, J. Bauersachs, B. Fisslthaler, R. Busse: Ca^{2+}-Independent Activation

of the Endothelial Nitric Oxide Synthase in Response to Tyrosine Phosphatase Inhibitors and Fluid Shear Stress. *Circ Res* 82, 686–695 (1998)
DOI: 10.1161/01.RES.82.6.686

88. B. J. Michell, Z-p. Chen, T. Tiganis, D. Stapleton, F. Katsis, D. A. Power, A. T. Sim, B. E. Kemp: Coordinated control of endothelial nitric-oxide synthase phosphorylation by protein kinase C and the cAMP-dependent protein kinase. *J Biol Chem* 276, 17625–17628 (2001)
DOI: 10.1074/jbc.C100122200

89. M. B. Harris, H. Ju, V. J. Venema, H. Liang, R. Zou, B. J. Michell, Z. P. Chen, B. E. Kemp, R. C. Venema: Reciprocal phosphorylation and regulation of endothelial nitric-oxide synthase in response to bradykinin stimulation. *J Biol Chem* 276, 16587–16591 (2001)
DOI: 10.1074/jbc.M100229200

90. R. Kou, D. Greif, T. Michel: Mechanisms of Signal Transduction : Dephosphorylation of Endothelial Nitric-oxide Synthase by Vascular Endothelial Growth Factor : Implications for the Vascular Responses to Cyclosporin A. *J Biol Chem* 277, 29669–29673 (2002)
DOI: 10.1074/jbc.M204519200

91. I. Fleming, B. Fisslthaler, S. Dimmeler, B. E. Kemp, R. Busse: Phosphorylation of Thr495 Regulates Ca^{2+}/Calmodulin-Dependent Endothelial Nitric Oxide Synthase Activity. *Circ Res* 88, e68–e75 (2001)
DOI: 10.1161/hh1101.092677

92. Q-K. Tran, J. Leonard, D. J. Black, A. Persechini: Phosphorylation within an autoinhibitory domain in endothelial nitric oxide synthase reduces the Ca^{2+} concentrations required for calmodulin to bind and activate the enzyme. *Biochemistry* 47, 7557–7566 (2008)
DOI: 10.1021/bi8003186

93. M. Matsubara: Regulation of Endothelial Nitric Oxide Synthase by Protein Kinase C. *J Biochem* 133, 773–781 (2003)
DOI: 10.1093/jb/mvg099

94. G. K. Kolluru, J. H. Siamwala, S. Chatterjee: eNOS phosphorylation in health and disease. *Biochimie* 92, 1186–1198 (2010)
DOI: 10.1016/j.biochi.2010.03.020

95. E. F. Pettersen, T. D. Goddard, C. C. Huang, G. S. Couch, D. M. Greenblatt, E. C. Meng, T. E. Ferrin: UCSF Chimera--A Visualization System for Exploratory Research and Analysis. *JComput Chem* 25, 1605–1612 (2004)
DOI: 10.1002/jcc.20084

96. M. Aoyagi, A. S. Arvai, J. A. Tainer, E. D. Getzoff: Structural basis for endothelial nitric oxide synthase binding to calmodulin. *EMBO J* 22, 766–775 (2003)
DOI: 10.1093/emboj/cdg078

97. K. Pervushin, R. Riek, G. Wider, K. Wüthrich: Attenuated T2 relaxation by mutual cancellation of dipole-dipole coupling and chemical shift anisotropy indicates an avenue to NMR structures of very large biological macromolecules in solution. *Proc Natl Acad Sci U S A* 94, 12366–12371 (1997)
DOI: 10.1073/pnas.94.23.12366

98. R. Riek, K. Pervushin, K. Wüthrich: TROSY and CRINEPT: NMR with large molecular and supramolecular structures in solution. *Trends Biochem Sci* 25, 462–468 (2000)
DOI: 10.1016/S0968-0004(00)01665-0

99. B. Vincent, N. Morellet, F. Fatemi, L. Aigrain, G. Truan, E. Guittet, E. Lescop: The Closed and Compact Domain Organization of the 70-kDa Human Cytochrome P450 Reductase in Its Oxidized State As Revealed by NMR. *J Mol Biol* 420, 296–309 (2012)
DOI: 10.1016/j.jmb.2012.03.022

100. C. Fernandez, G. Wider: TROSY in NMR studies of the structure and function of large biological macromolecules. *Curr Opin Struct Biol* 13, 570–580 (2003)
DOI: 10.1016/j.sbi.2003.09.009

101. M. Mund, J. H. Overbeck, J. Ullmann, R. Sprangers: LEGO-NMR Spectroscopy : A Method to Visualize Individual Subunits in Large Heteromeric Complexes. *Angew Chem Int Ed Engl* 52, 11401–11405 (2013)
DOI: 10.1002/anie.201304914

102. H. N. Zhu, S. Q. Pan, S. Gu, E. M. Bradbury, X. Chen: Amino acid residue specific stable isotope labeling for quantitative proteomics. *Rapid Commun Mass Spectrom* 16, 2115–2123 (2002)
DOI: 10.1002/rcm.831

103. D. W. Hoffman, L. D. Spicer: *Isotopic Labeling of Specific Amino Acid Types as an Aid to NMR Spectrum Assignment of the Methionine Repressor Protein*. (1991)

104. N. R. Skrynnikov, F. A. A. Mulder, B. Hon, F. W. Dahlquist, L. E. Kay: Probing slow time scale dynamics at methyl-containing side chains in proteins by relaxation dispersion NMR measurements: Application to methionine residues in a cavity mutant of T4 lysozyme. *J Am Chem Soc* 123, 4556–4566 (2001)
DOI: 10.1021/ja004179p

105. H. Duewel, E. Daub, V. Robinson, J. F. Honek: Incorporation of Trifluoromethionine into a Phage Lysozyme: Implications and a New Marker for Use in Protein ^{19}F NMR. *Biochemistry* 36, 3404–3416 (1997)
DOI: 10.1021/bi9617973

106. J. K. Mcdonald, C. M. Taylor, S. Rafferty: Design, preparation, and characterization of mixed dimers of inducible nitric oxide synthase oxygenase domains. *Protein Expr Purif* 27, 115–127 (2003)
DOI: 10.1016/S1046-5928(02)00588-0

107. T. J. Dolinsky, J. E. Nielsen, J. A. McCammon, N. A. Baker: PDB2PQR: An automated pipeline for the setup of Poisson-Boltzmann electrostatics calculations. *Nucleic Acids Res* 32, W665–W667 (2004)
DOI: 10.1093/nar/gkh381

108. T. J. Dolinsky, P. Czodrowski P, H. Li, J. E. Nielsen, J. H. Jensen, G. Klebe, N. A. Baker: PDB2PQR: Expanding and upgrading automated preparation of biomolecular structures for molecular simulations. *Nucleic Acids Res* 35, W522–W525 (2007)
DOI: 10.1093/nar/gkm276

109. J. Kyte, R. F. Doolittle: A simple method for displaying the hydropathic character of a protein. *J Mol Biol* 157, 105–132 (1982)
DOI: 10.1016/0022-2836(82)90515-0

Key Words: Nitric Oxide Synthase, Calmodulin, Protein dynamics, NMR spectroscopy, Amide exchange, Review

Send correspondence to: Joseph Guy Guillemette, Department of Chemistry, University of Waterloo, Waterloo, Ontario N2L 3G1, Canada, Tel: 519-888-4567 ext. 35954, Fax: 519-746-0435, E-mail: jguillem@uwaterloo.ca